Research Article

Rapid Adaptation of Cellular Metabolic Rate to the MicroRNA Complements of Mammals, and its Relevance to the Evolution of Endothermy

Bastian Fromm, PhD
The Arctic University Museum of Norway
UiT- The Arctic University of Norway
9037 Tromsø, Norway

and

Thomas Sorger, PhD*
Department of Biology
Roger Williams University
Bristol, Rhode Island 02809, USA

* corresponding author

SUMMARY

Terrestrial mammals range in size over six orders of magnitude, but metabolic rate/cell *(sMR*) varies only ~ 5-fold, constrained by the matching of protein synthesis (20% *sMR*) to cell size. Based on energy efficiency, we hypothesized that *sMR* varies in proportion to the global repression of translation by microRNAs. With the number of microRNA families (*miRNA.Fam*) as predictor, an Ornstein-Uhlenbeck process of stabilizing selection, together with an adaptive shift between Atlantogenata and Boreoeutheria, accounted for 95% of the variation in optimally scaled *sMR*. Relative to mass, branchwise rates of evolution of *sMR*, *miRNA.Fam* and body temperature, increased 7- to 10-fold. *sMR* variation was also predicted by the total energy cost of all model conserved microRNA-target interactions. Optimal allometric scaling of the *sMR-miRNA.Fam* relationship depended on body temperature and approached field metabolic rate in Boreoeutheria, consistent with the heat dissipation model of Speakman and Król (2010).

INTRODUCTION

The resting metabolic rate (*rMR*) and body mass of mammals have evolved in tandem according to a conserved allometry (Kleiber, 1932; Brody and Proctor, 1932; Savage et al, 2004; White et al, 2006; McNab, 2008; McNab, 2009; Naya et al, 2013a; Gillooly et al, 2017; Ballesteros et al, 2018; McNab, 2019) that has limited the range of the ratio rMR/M^{exp}, or specific *MR* (*sMR*) (White et al, 2019 and Supplementary Figure S1). Since cellular *MR* accounts for 90% of *sMR* (Rolfe and Brown, 1997), the 10^6-fold range in the mass of terrestrial mammals represents, to a first approximation, variation in the total number of cells with highly conserved cell size and cellular *MR*.

An important constraint on cellular *MR* is the cell cycle-related coupling of macromolecular synthesis and cell size in mammalian cells, as in yeast cells (Ginzberg et al, 2018; Knapp et al, 2019; Neurohr et al, 2019) (for reviews, see Björklund, 2019 and Zatulovskiy and Skotheim, 2020). Matching of the rate of protein synthesis to cell size is predicted by models in which the rate of translation in exponentially growing cells is limited by competition among mRNAs for ribosomes (Kafri et al, 2016; Lin and Amir, 2018). A slow rate of translation relative to transcription minimizes energy losses due to both error correction by kinetic proofreading (Hopfield, 1974; Ninio, 1975; Bennett, 1979; Barato and Seifert, 2015; Banerjee et al, 2017; Mallory et al, 2019; Yu et al, 2022), and to intrinsic translation noise (Ozbudak et al, 2002; Lin and Amir, 2021). This adaptation can be understood in light of the 10- to 100-fold higher thermodynamic cost per gene of translation relative to transcription in eukaryotes (Wagner, 2005; Lynch and Marinov, 2015). Absent the evolution of compensatory mechanisms, the fitness benefits associated with the evolution, in late-branching placental mammals, of faster cellular *MR*s, higher body temperatures and permanent homeothermy would have been offset by increasingly noisy and error-prone translation. Assuming selection against energy inefficiency, we postulated that cellular MR would vary directly with the global attenuation of intrinsic translation noise by microRNA activity (Bartel and Chen, 2004; Hornstein and Shomron, 2006;

Schmiedel et al, 2015; Bartel, 2018). This expectation was met by the number of conserved microRNA families (*miRNA.Fam*).

Unlike the impact of other regulators of gene expression, the global repression of translation by total combinatorial microRNA activity (hereafter "*global microRNA activity*") has an obligatory effect on *sMR*, by decreasing the overall rate of translation (Krek et al, 2005; Baek et al, 2008; Selbach et al, 2008; Friedman et al, 2009). Changes in the rate of translation disproportionally affect *sMR*, since protein synthesis, which drives 20% of ATP turnover (Buttgereit and Brand, 1995), is the single most costly and least efficient cellular metabolic process (Rolfe and Brown, 1997). Assuming conservatively that global microRNA activity reduces the global rate of translation by 25% (Krek et al, 2005; Baek et al, 2008; Selbach et al, 2008; Spies et al, 2013; Schmiedel et al, 2015; Lu et al, 2023), a 10-fold increase in cellular *MR*, without a corresponding increase in global microRNA activity, would incur a 6% loss of efficiency of cellular *MR* (5.4% of overall *rMR*) due to protein overproduction, as well as add to the cost of protein degradation (Peth et al, 2013; Snoberger et al, 2017). While not directly comparable, it is worth noting that losses of fitness of up to 3% were found when the intrinsic translation noise of individual, constitutive proteins in yeast was doubled (Schmiedel et al, 2019).

Indeed, the rates of translation of low- and high-abundance transcripts in mammalian cells appear to have evolved under an energy constraint and conform to the predicted outcome of global microRNA activity (Vogel et al, 2010; Schwanhäusser et al, 2011). MicroRNAs preferentially repress low-abundance mRNAs (Bartel and Chen, 2004; Schmiedel et al, 2015) which, owing to suboptimal ratios of rates of translation/ transcription, are more costly to translate than highly abundant mRNAs (Schwanhäusser et al, 2011). The latter are also enriched in the transcripts of housekeeping genes, and encode proteins that tend to be shorter and more stable (Eisenberg and Levanon, 2003).

In previous studies, the evolutionary constraint on the ratio of *MR* to mass has been inferred from the analysis of the co-variation of the individual traits fit to models separately (Venditti et al, 2011; Baker et al, 2015; Avaria-Llautureo et al, 2019; White et al, 2019). Here we implement allometric scaling by maximum likelihood in order to directly test the ratio rMR/M^{exp} in models of dependence on *miRNA.Fam*, body size and body temperature (T_b), and demonstrate that it is both more robust to variation in mass and more sensitive to the ratio of surface area/mass. Specifically, we ask whether the similar pattern of variation between *sMR* and *miRNA.Fam* better reflects phylogenetic distance (Brownian motion model) or the outcome of stabilizing selection (Ornstein-Uhlenbeck model) (Bartoszek et al, 2012), and at which stage of mammalian evolution an adaptive shift (Bastide et al, 2018) would have been most likely to simulate the parallel increases in *sMR* and *miRNA.Fam*. We infer branch-wise rates of evolution of *sMR.75*, log mass, *miRNA.Fam*, and T_b to test for selection (Baker et al, 2016), and compare conventional and variable rate phylogenetic regression models to test for trait independence. Since the global attenuation of intrinsic

translation noise also depends on the density of 3'-UTR target sites and their sensitivity to the combinatorial action of microRNAs, we compare the variation in *sMR* to the variation in energy saving per cell, estimated from all of the model interactions between conserved microRNAs and their conserved target sites. Finally, we consider the implications of the higher surface area dependence of optimal *sMR* scaling among high-T_b Boreoeutheria, in light of the theory that variation in mammalian metabolic rates is limited by the maximum rate of heat dissipation (Speakman and Król, 2010).

RESULTS

The acquisition of microRNA families accelerated in late-branching mammals

The number of families of conserved, microRNA-encoding genes (*miRNA.Fam*) increased steadily in the order of divergence of vertebrate clades, except among Archosauria (Figure 1A)(Fromm et al, 2020; Álvarez-Carretero et al, 2022). The variation in *miRNA.Fam* was unrelated to genome size or number of coding genes (Supplementary Table S2), but was 87% correlated with *sMR.80* ($rMR/M^{0.80}$) across 16 non-avian vertebrates (P = 2.20e-16, Spearman rank correlation) (Figure 1B).

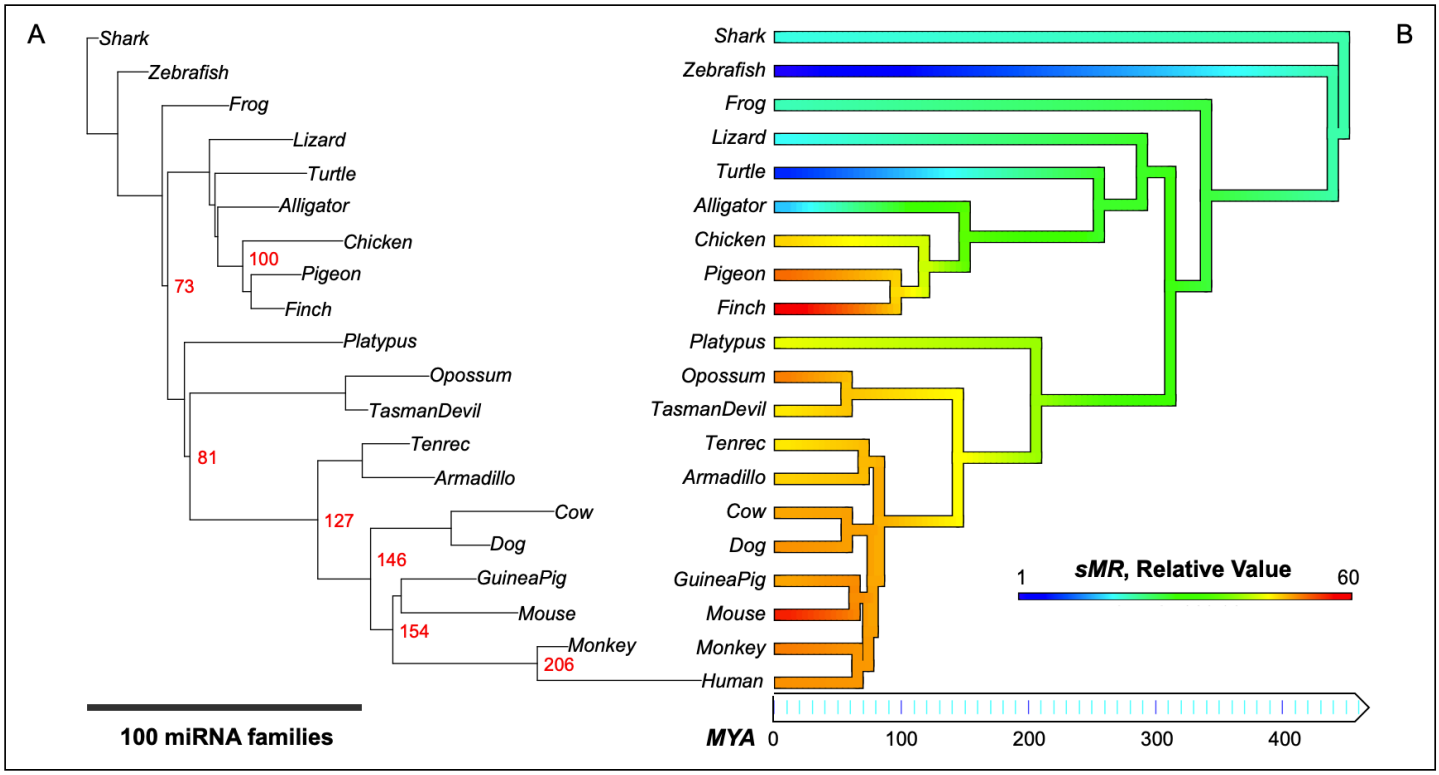

Figure 1. Evolution of the number of microRNA families and cellular metabolic rate (*sMR*).

A. Distance tree of microRNA families. Branch lengths represent the total number of families. Node values represent the number of shared microRNA families in each clade.

B. The log ratios of *sMR*s ($rMR/M^{0.80}$) were scaled to the original range of *sMR* and mapped onto the vertebrate phylogeny. Divergence times were drawn from Álvarez-Carretero et al 2022) for mammals, and Irisarri et al (2017) for earlier-branching vertebrates.

The acquisition of shared microRNA families accelerated in placental mammals, with increases of 46 in the 64 million years between the divergences of Theria and Placentalia, and 27 in the 8.7 million years between the divergence of Atlantogenata and Euarchontoglires (Álvarez-Carretero et al, 2022). Among the latter, fewer than ten microRNA families are uniquely expressed in the placenta (Fromm et al, 2020). These differences correspond to gains of 0.92% per million years in pre-placental mammals *versus* 2.24% per million years among placentalia. Consequently, the number of microRNA families common to all four Euarchontoglires (154) is approximately twice the number shared by all Theria (81), as is the number of genes (Figure 1A) (Fromm et al, 2020).

Allometric scaling of vertebrate MRs by maximum likelihood

In conventional studies of the evolution of metabolic rate, constraints such as mass, temperature, aridity, and diet have been inferred from the slope and residual analysis of the regression of log *rMR* on log *M* (see, for example, Kleiber, 1932; McNab, 2008; McNab, 2009; Naya et al, 2013a; Ballesteros et al, 2018; McNab, 2019). We first established that our sample of 20 vertebrate species in MirGeneDB was broadly representative of vertebrates with regard to the distributions of mass and *rMR*. As shown in Figure 1A, the *rMR*s of the 14 endotherms and 6 ectotherms exhibited a conserved relationship to mass, with slopes (0.75 and 0.88 respectively) very similar to those reported in previous, large-scale studies (White et al, 2006; Gillooly et al, 2017). When M^{exp} was fit by maximum likelihood to the distribution of *rMR* (with resolution $M^{0.1}$) (White, 2011), the optimal regression yielded a common slope

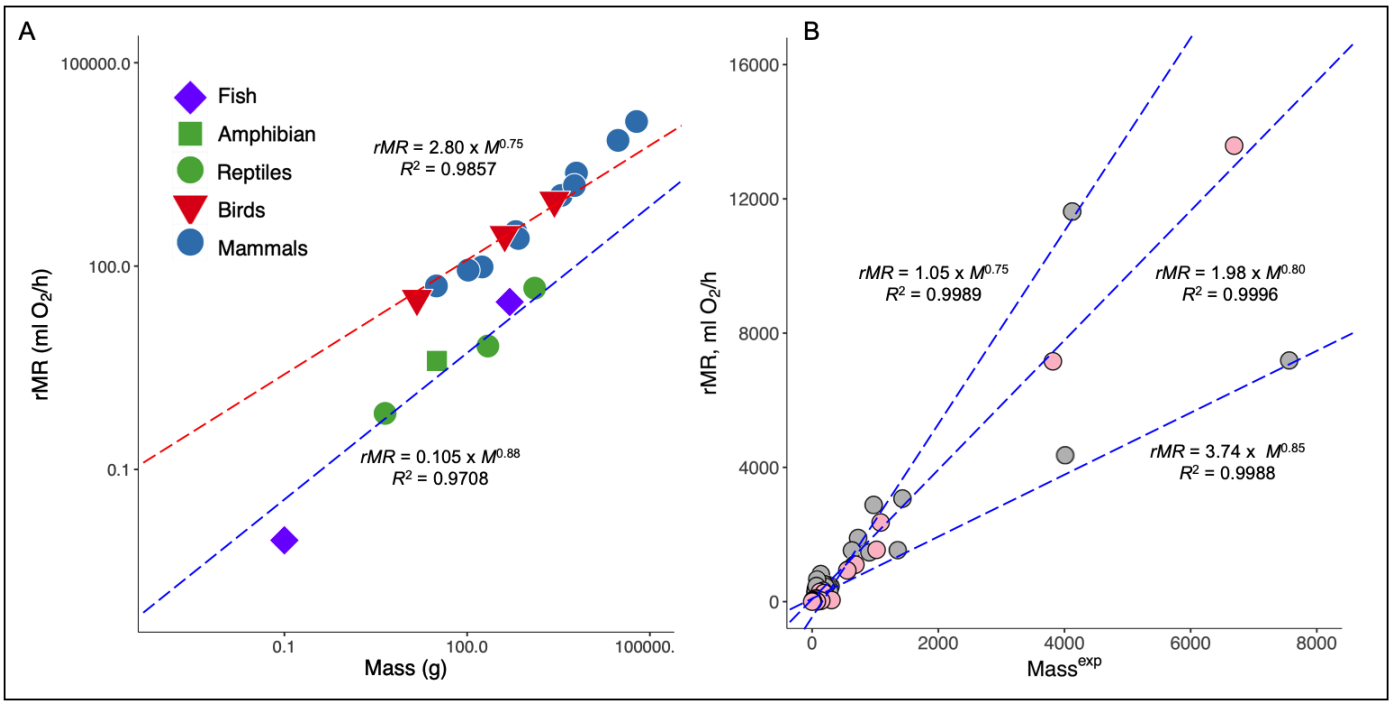

Figure 2. Comparison of the allometric scaling of the *sMR*s of 20 vertebrates by (A) the conventional power law method, or (B) maximum likelihood scaling according to the optimal fit ($M^{0.80}$: pink circles) and two suboptimal fits ($M^{0.75}$, $M^{0.85}$: gray circles).

of 0.80 for both ectotherms and endotherms, normally distributed residuals, and a smaller residual error than the log-based method for either endotherms or ectotherms (*P* = 6.36e-32) (Figure 1B).

Importantly, even though the relationship of *rMR* to M^{exp} is heteroscedastic (Figure 2B), when the scaling of M^{exp} is optimized in order to match the ratio of rMR/M^{exp} to the distribution of a third covariate, such as such as *miRNA.Fam*, the variation is homoscedastic (Figure 3 and Supplementary Figure S3), and therefore suitable for comparing the *sMR* dependence on covariates in species ranging in size over several orders of magnitude (Benson et al, 2022).

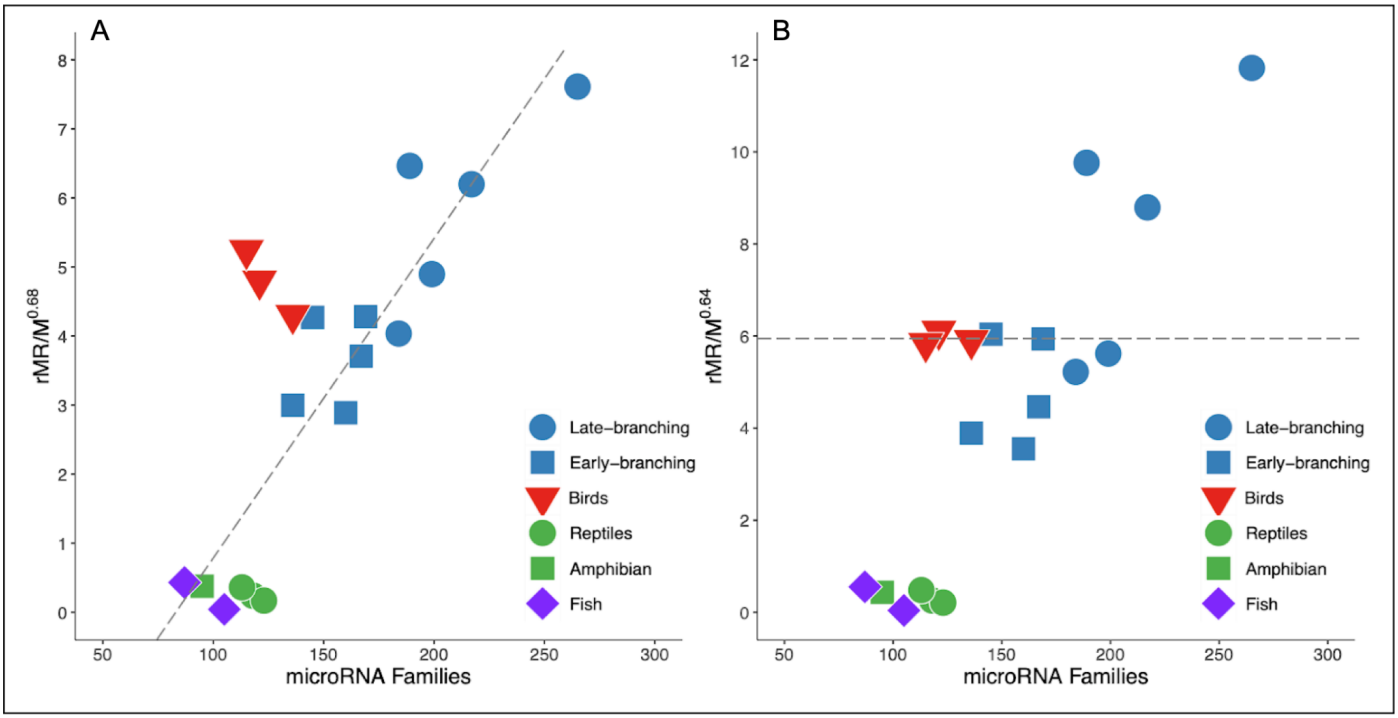

Figure 3. Phylogenetic regression of *sMR.68* ($rMR/M^{0.68}$) on *miRNA.Fam*.

A. The number of microRNA families in non-avian tetrapods accounted for 84% of the variation in *sMR*68, independent of phylogenetic distance (see Supplementary Table S2).
B. The same data scaled to the slope of log *rMR*/log mass (0.64) in 211 birds (Fristoe et al, 2015).

Tetrapod sMRs are correlated with the number of microRNA families, independent of phylogenetic distance or size

Phylogenetic linear regression (assuming uniform rates of evolution) indicated that the distribution of *miRNA.Fam* across 14 non-avian tetrapods accounted for 84% of the variation in optimally scaled *sMR* ($rMR/M^{0.68}$, *P* = 2.26e-06) (Figure 3A), independent of phylogenetic distance (Pagel's *lambda* = 0.00). The optimal allometric slope, 0.68, was significantly different from 0.78, the slope of log rMR/log *M* (*P* = 8.02e-03, ANCOVA) (Supplementary Table S2). The variation with respect to the number of microRNA genes was weaker and secondary to phylogeny (Pagel's *lambda* = 1.0). Similar results were obtained when only mammals were considered, with an optimal slope of 0.71 with respect to *miRNA.Fam*, compared to 0.77 for log *rMR*/log *M* (Supplementary Table S2).

The previous analysis excluded the three bird species in our sample (chicken, dove and finch) since the absolute number of avian microRNA families decreases in phylogenetic order (Figure 1A). However in large datasets, the log-based allometric exponent for *rMR* in birds is markedly lower than that found in mammals, *e.g.* $M^{0.64}$ *versus* $M^{0.73}$ (White et al, 2006; Fristoe et al, 2015). When scaled to $M^{0.64}$, the slope of the regression of the bird *sMRs* on the number of miRNA families was 0.00 (Figure 3B), and turned positive for any allometric exponent < 0.64. That is, when scaled with an allometric exponent < 0.64, bird *sMR*s do vary positively with *miRNA.Fam*. Thus, the optimal allometric scaling of *sMR* with respect to *miRNA.Fam* in birds may be displaced toward a greater dependence on surface area *i.e.* lower allometric exponent, relative to the slope of log *rMR*/log mass, as we have found in mammals (Supplementary Table S2).

As the basis for modeling *sMR* in relation to a third covariate, maximum likelihood scaling across the arithmetic range of *rMR* is more sensitive than the log-based method to the ratio of surface area/mass, and therefore provides more information regarding the biophysical nature of the relationship. For example, when scaled by maximum likelihood, the optimal slopes of *sMR* with respect to *miRNA.Fam* for early- ($M^{0.78}$) and late-branching mammals ($M^{0.70}$) were significantly different (P = 1.54e-02) (Supplementary Table S2 and Supplementary Figure S2). However, when the *sMR*s were derived from the slopes of log *rMR*/log *mass* ($M^{0.75}$ and $M^{0.74}$, respectively) for comparison with *miRNA.Fam*, the difference between these groups was not significant (P = 0.2240, ANCOVA).

Since the acquisition of microRNAs in increase in *sMR* in mammals were associated with higher body temperatures and generally larger body size (Baker et al, 2015), we used two approaches to dissect the interdependencies among these three traits. Conventional analysis of covariance indicated that the dependence of *sMR.71* on *miRNA.Fam* in mammals was still significant after controlling for mass (P = 4.58e-02), but not after controlling for body temperature (P = 0.4069). To better understand the interaction between the *sMR.71-miRNA.Fam* relationship and body temperature, we conducted a sliding window analysis that revealed a significant anti-correlation between the optimal *sMR* exponent and body temperature across samples of five mammals composed of 0 - 5 late-branching mammals (Figure 4) (P = 2.01e-02). In other words, as mean T_b increased, the relationship of *sMR* to *miRNA.Fam* became more dependent on surface area, *i.e.* a lower optimal allometric exponent.

This analysis also demonstrated why allometric scaling of *sMR* by maximum likelihood is more robust to variation in mass than inference from the slope log *rMR*/log *M*. As the mean temperature of each sample increased, average mass, and the slope of log *rMR*/log *M*, initially decreased and then increased (Figure 4). In contrast, the slope of the optimal scaling with respect to *miRNA.Fam* decreased continuously with temperature (Figure 4). Being more robust to variation in mass and more sensitive to temperature, the ratio of surface area/mass indicated by optimal scaling is likely to be

relevant when comparing species that have different rates of heat generation and dissipation (Naya et al, 2013b; Fristoe et al, 2015; Ballesteros et al, 2018).

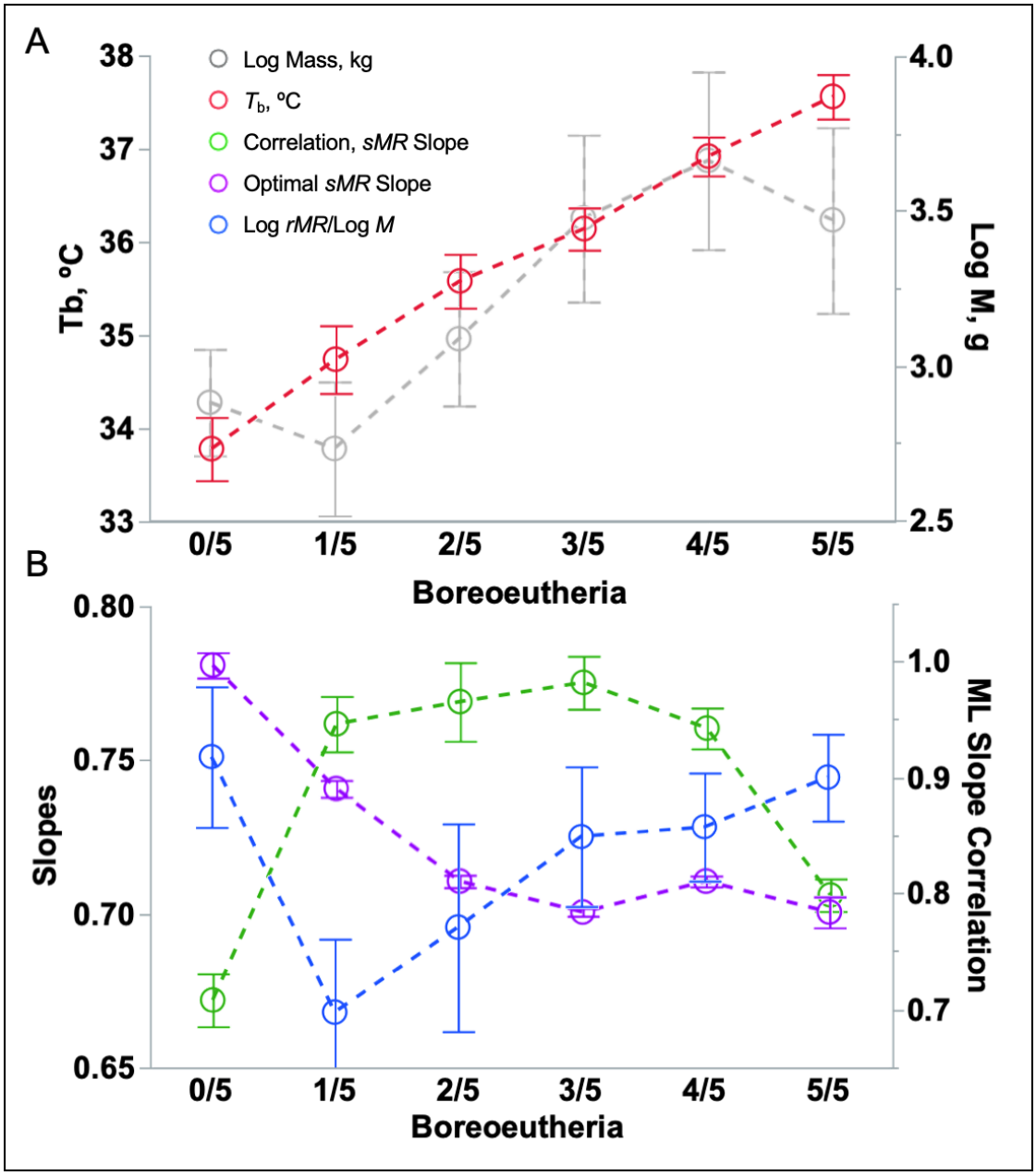

Figure 4. Sliding Window Analysis of the sensitivity and robustness of allometric scaling of *sMR* by maximum likelihood. Ten mammals were ranked by temperature. Successive groups of five were designated by the number of Boreoeutheria.
A. The effect of group composition on the mean value of body temperature or log mass.
B. The effect of group composition on the slope of log rMR/log M, the optimal slope of rMR/M^{exp} with respect to *miRNA.Fam* and the corresponding correlation coefficient. Values represent mean ± ½ standard error of the mean).

Cellular MR variation in relation to the number of microRNA families conforms to an OU model of stabilizing selection

We compared two hypotheses for the evolution of metabolic rates in relation to the microRNA complement: a Brownian motion (BM) process, where *sMRs* diverge as a function of phylogenetic distance, *versus* an Ornstein-Uhlenbeck (OU) process, according to which *sMR*s, under the influence of stabilizing selection, converge asymptotically toward the distribution of an independently varying predictor (Bartoszek et al, 2012), in this case, the number of microRNA families. We applied two complementary methods in order to test these models: first, we compared how well each process fit the relationship of *sMR* to *miRNA.Fam* across the range of allometric exponents 0.66 - 0.80; second, using the same phylogeny and distribution of microRNA families, we compared the actual distribution of *sMR* values with those generated by BM and OU simulations that included an adaptive shift at different stages of mammalian evolution.

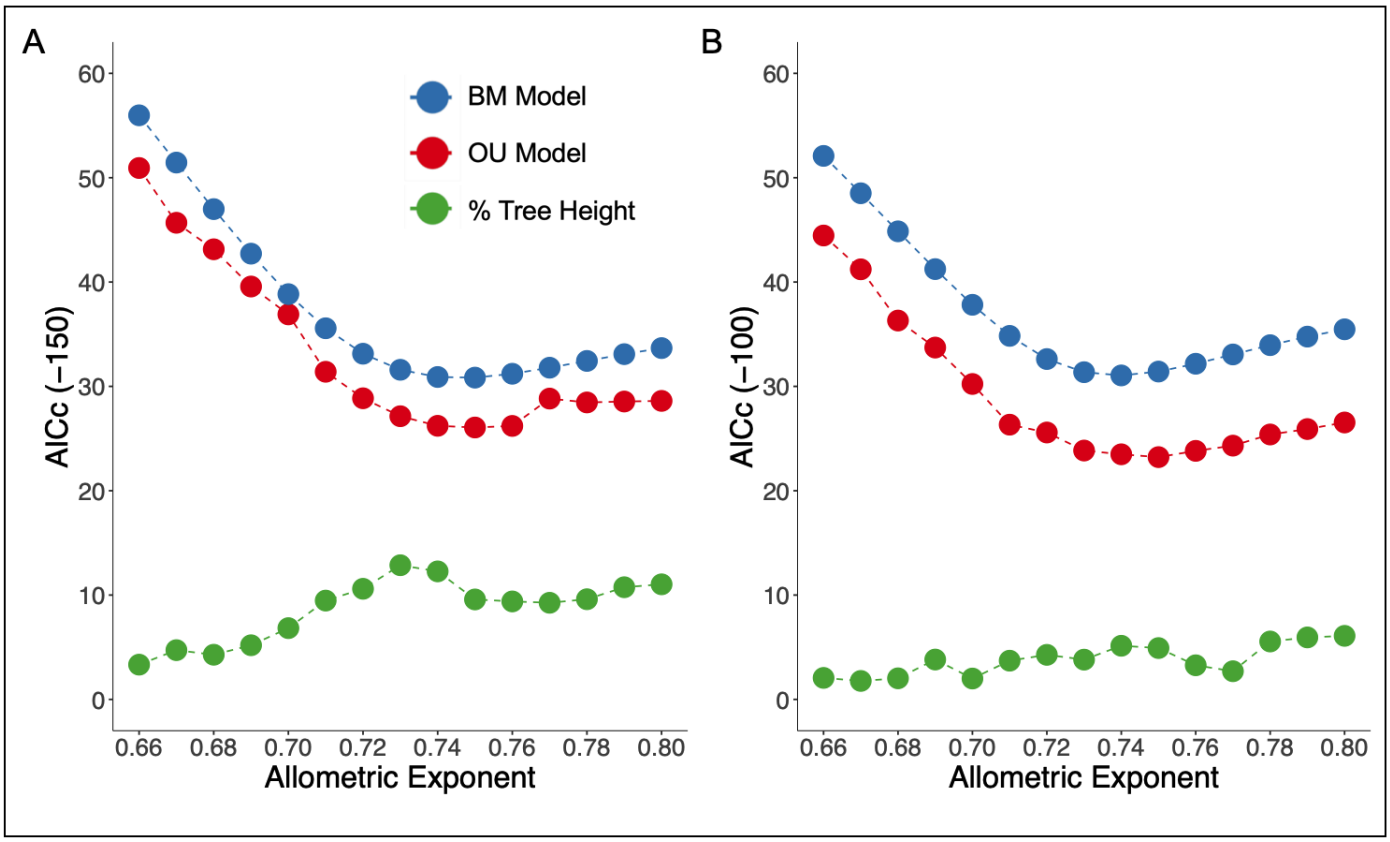

Figure 5. Comparison of BM and OU models for the variation of s*MR* with respect to *miRNA.Fam* across 14 tetrapods (A) or 10 mammals (B). Curves represent the corrected values of the Akaike information criterion (AICc) for each model, and the rate of adaptation (% tree height) for the OU models. Note the difference in range of the ordinate axes.

For any *sMR* scaling in the range $M^{0.66}$ - $M^{0.80}$, the BM model for the evolution of *sMR* with respect to *miRNA.Fam* was inferior to the OU model (Figure 5A): at $M^{0.75}$, the ΔAICc (BM-OU) value was +2.68 before correction (Supplementary Figure S4) and +6.88 after empirical correction of the bias recorded in 40 OU and 40 BM simulations on the same phylogenetic tree (Supplementary Table S3). The inferred

rate of adaptation of *sMR* with respect to *miFam* at $M^{0.75}$ corresponded to 12.63% of the tetrapod tree (Figure 4A), or 4.92% when only the 10-mammal tree was considered (Figure 5B). Specific *MR*s exhibited a similar ΔAICc optimum with respect to the number of microRNA genes (*mirGen*), albeit with smaller differences in the ΔAICc between the OU and BM models (Supplementary Figure S5). However no such inflection was observed in models of *sMR* variation in relation to genome size (*Gnm*) or number of coding genes (*Cdg*), and AICc values declined monotonically (Supplementary Figure S4).

In our dataset there was an abrupt increase in the number of microRNA families between the two Atlantogenata (Tenrec: 160, Armadillo: 169) two Laurasiatheria (Dog: 184; Cow: 212), reminiscent of a Simpsonian 'jump' (Simpson, 1944). We therefore simulated the evolution of *sMR* with respect to *miRNA.Fam* in 14 tetrapods by either a BM or OU process, assuming two adaptive shifts (Bastide et al, 2018): the first corresponding to the divergence of mammals, and the second shift corresponding to the divergence of either Placentalia, Boreoeutheria, or Euarchontoglires (Figure 6A) .

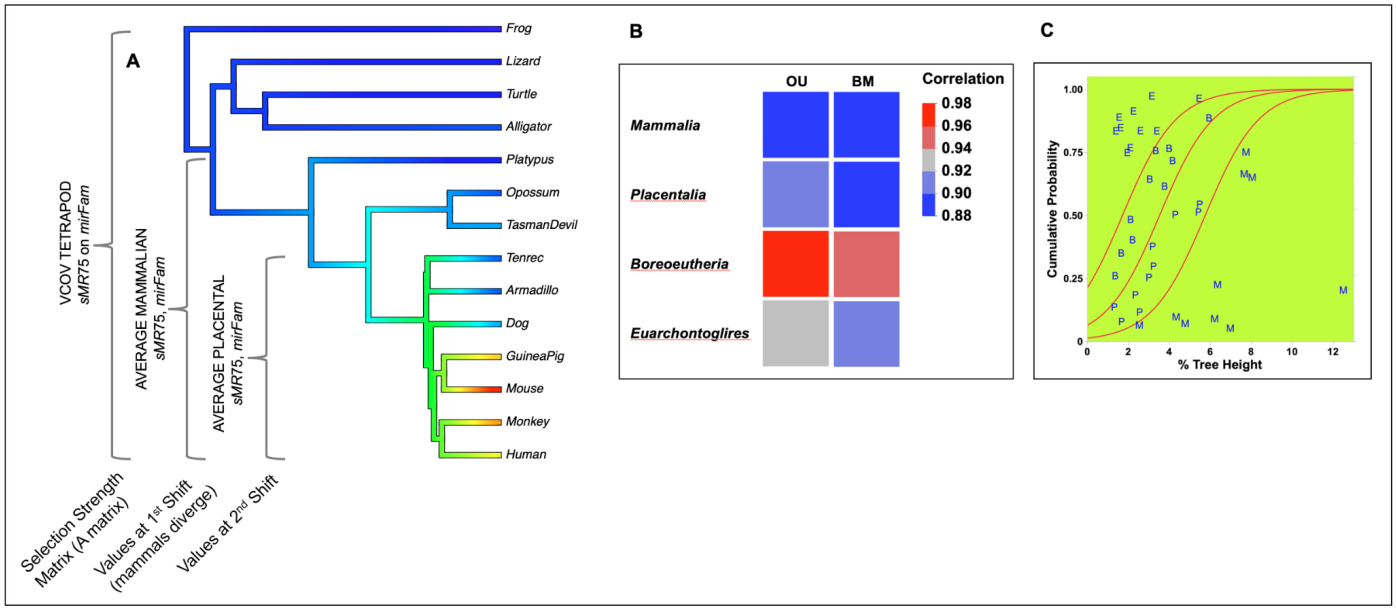

Figure 6. Design and analysis of simulated adaptive shifts in the evolution of *sMR* in relation to the predictor *miRNA.Fam.*

A. The variance/covariance matrix for the regression of *sMR.75* on *microRNA families* was used as the selection strength matrix to generate pairs of values for these traits. The average values of these traits across all mammals, or across placental mammals, were assigned to the first shift (divergence of mammals) and second shift, respectively. Phenogram colors correspond to the log of the *sMR.75* values scaled to the original, 36-fold range. B. Correlations with the actual *sMR.75* distribution of the average of ten simulations of the OU or BM process in 14 tetrapods. Adaptive shifts were modeled at the divergence of Mammalia (single shift), with a second shift at the divergence of either Placentalia, Boreoeutheria or Euarchontoglires (*P* = 1.23e-05 for OU *versus* BM, Boreoeutheria shift). C. Validation of the estimated rates of adaptation: prediction of shift positions according to the % tree height obtained from ten OU models. Shift positions are indicated by the first letter of each diverging clade (M, P, B, E). *P* = 5.19e-06 (ordinal logistic regression).

OU and BM models simulated the biphasic evolution of *sMR* in mammals most precisely when this was scaled to $M^{0.75}$ (Supplementary Figure S5). The best model, an OU process with an adaptive shift at the divergence of Boreoeutheria, accounted for 95% of the variation in *sMR.75* (P = 4.10e-09), compared to 88% for the corresponding BM model (Figure 6B). Estimates of the rate of adaptation increased in the order of the phylogenetic position of the second adaptive shift, corresponding to decreasing distance from the tips of the phylogenetic tree (P = 5.19e-06, ordinal logistic regression) (Figure 6C).

In sum, for both OU and BM models of the variation in *sMR* across mammals, the optimal allometric scaling with respect to *miRNA.Fam* corresponds closely to the conserved ¾ power law model for the overall dependence of *rMR* on mass in mammals. It remains to be determined whether in birds, by analogy, the optimal *sMR* scaling in BM and OU models of *sMR* dependence on *miRNA.Fam* corresponds to the ~ ⅔ power law model that fits avian resting metabolic rates (White et al, 2006; Fristoe et al, 2015; Ballesteros et al, 2018).

The divergence of Boreoeutheria was associated with acceleration in the rates of evolution of *sMR.75, miRNA.Fam and body temperature.*

Based on the evidence for an adaptive shift in the dependence of *sMR* on *miRNA.Fam* and its relationship to body temperature, we anticipated increases in the branch-wise rates of evolution of all three traits (Baker et al, 2015), independent of any change in the rate of evolution of mass, as previously indicated by analysis of covariance.

Using a Bayesian variable rates algorithm, we generated phylogenetic trees in which branch lengths were scaled in proportion to the rate of directional evolution of a singe trait, relative to an expectation of a Brownian motion process (Venditti et al, 2011; Baker et al, 2016) (Figure 7). The variable rate trees representing *sMR.75*, *miRNA.Fam*, T_b and mass were strongly supported (Bayes factor > 5) (Raftery, 1996; Baker et al, 2016), based on comparison of the median log likelihood of the 100 trees with the greatest (1%) likelihood and the 100 trees with the smallest (1%) sum of adjustments to branch lengths, *i.e.* those trees most similar to the reference constant rate model. In the variable rate trees for *sMR.75*, *miRNA.Fam* and T_b, the branch lengths representing the descent of Primates from Theria were 99% correlated (Supplementary Table S4), and the lengths of the branch representing the relative rate of evolution between Atlantogenata and Boreoeutheria were 6.8 - 10 times the length of the branch representing the evolution of mass (Figure 7).

Our hypothesis predicts that compensatory noise suppression by microRNAs should be proportional to body temperature, since temperature is the primary determinant of the rate of protein synthesis, and therefore of intrinsic stochastic translation noise (Thattai and van Oudenaarden, 2001; Ozbudak et al, 2002). We adopted two complementary approaches in order to determine whether the dependence of

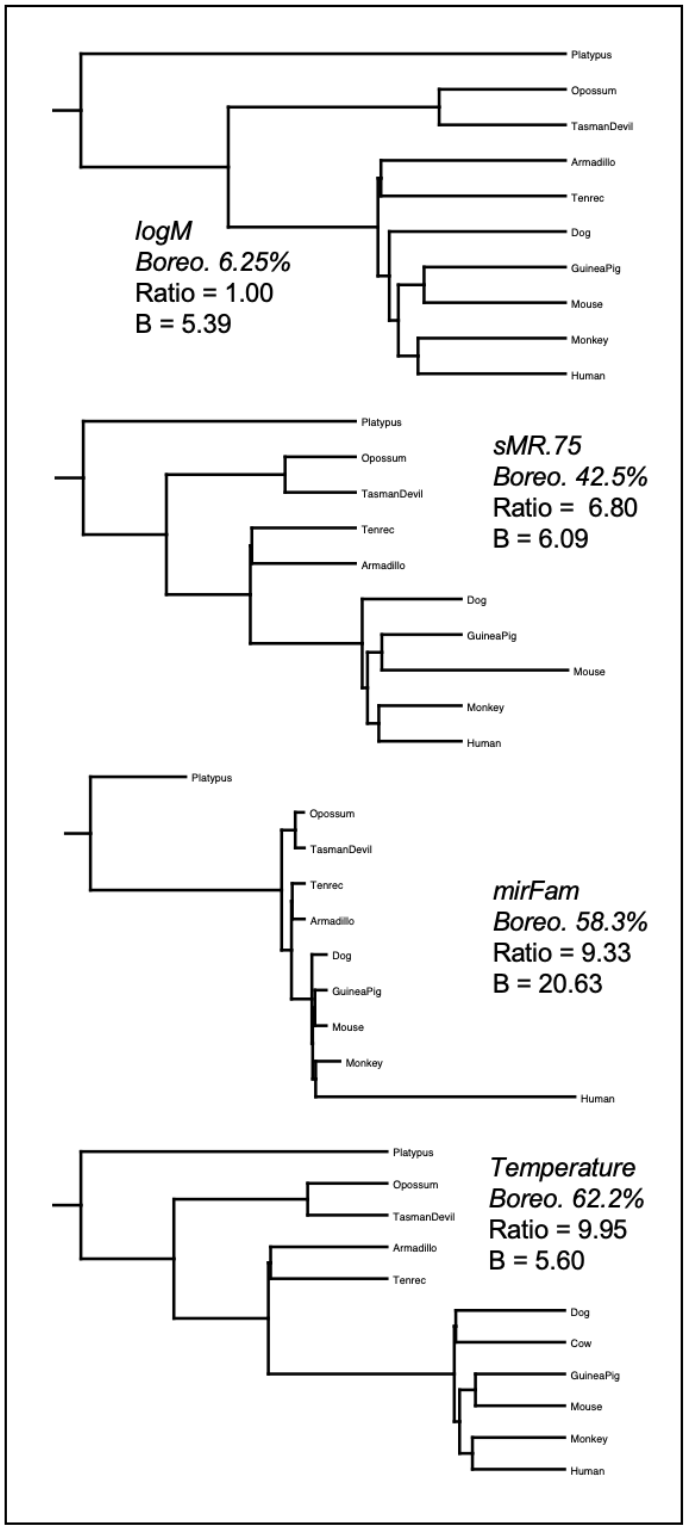

Figure 7. The ultrametric phylogeny of mammals was rescaled according to the rate of evolution of each of four traits. The length of the branch for the divergence of Boreoeutheria was compared (%) to the distance between the divergence of Theria and the divergence of Primates. Bayes factors were computed by comparing the median log likelihoods of these 100 trees with the median log likelihoods of the trees with the smallest sum of changes of scale, *i.e.* trees that differed the least from the constant rate model. The cow was included in the variable rate tree for temperature in order to to be able to infer the temperatures at the internal nodes (below).

sMR.75 on *miRNA.Fam* was secondary to body size or body temperature. As previously shown for *sMR.71*, analysis of covariance revealed that the dependence of *sMR.75* on *miRNA.Fam* was still significant after accounting for its dependence on size (log mass) (P = 2.67e-02), but not when controlling for body temperature (P = 0.2133). We also compared Bayesian regression models for the dependence of *sMR.75* on *miRNA.Fam* using the best 100/10,000 variable rate trees for *sMR.75*. When mass was included in the model, the overall relationship strength (R^2 = 0.63) was unchanged but the regression coefficient for mass dropped below zero in the majority of the models and the corresponding Bayes factor decreased from 3.13 to 2.38. On the other hand, when the model included body temperature, the majority of models had a positive regression coefficient for body temperature and the overall fit improved (R^2 = 0.67), as did the Bayes factor (3.20) (Supplementary Table S5).

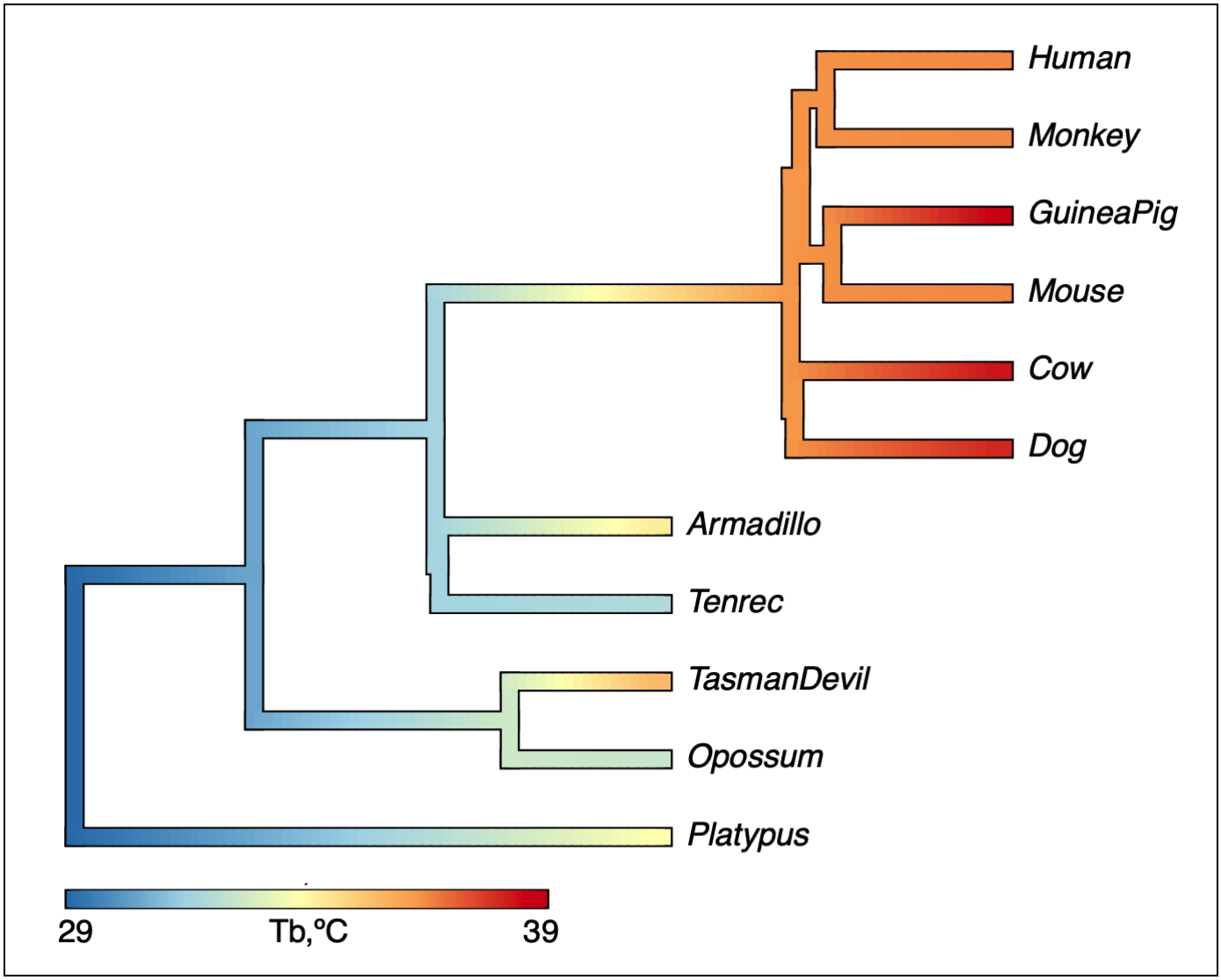

Figure 8. Bayesian reconstruction of ancestral body temperatures. The reference phylogeny was rescaled according to the rates of T_b evolution and ancestral node values were inferred in a Brownian motion context after fixing of the optimal ancestral mammalian T_b (29°C). The values at each node represent the median estimates for the 64/6,400 trees with the greatest likelihood (Brownian motion variance = 0.26°C).

Given that in large mammalian trees, changes in mammalian basal *MR* were not generally associated with changes in T_b, and that T_b decreased in more branches than increased (Avaria-Llautureo et al (2019), we considered the possiblity that the difference in T_b between the two early-branching (average T_b = 33.25°C) and six late-branching placentals (average T_b = 37.75°C) reflected opposite trajectories from a common, warmer-bodied ancestor. Using the 100 (1%) best variable rate trees for body temperature, Bayesian reconstruction of the temperatures at the ancestral nodes did not detect cooling of body temperature in any descendent clade. Instead, the difference in T_b between Atlantogeneta and Boreoeutheria could be attributed to a jump in body temperature in the most recent common ancestor of Boreoeutheria (Figure 8).

Faster sMRs and homeothermy in late-branching placental mammals are associated with the number, not kind, of microRNAs, and their conserved 3'-UTR targets

Of 146 microRNA families common to all six Boreoeutheria in this study, 19 were not shared by both Atlantogenata, tenrec and armadillo: 10 were present only in tenrec, 8 were present only in armadillo, and only a single microRNA family, miR-370, was absent from both genomes. Moreover, for three of these 19 microRNAs there were no conserved target sites: miR-105, miR-370 and miR-6715 (Supplementary Table S6). It cannot be excluded that the difference in energy regimes between early- and late-branching placental orders is related to the activities of some combination of the remaining 16 microRNAs, affecting targets unique to, or differentially expressed in later-branching placental mammals (Christmas et al, 2023); however, any such discovery would not shed light on the central question of this study, the nature of the broad correlation across mammals between cellular metabolic rate, the size of the microRNA repertoire, and the predicted number of microRNA-target interactions.

Our hypothesis assumes that global repression of translation by the combinatorial activity of microRNAs is proportional to the number of microRNA-target interactions and their sensitivity to repression. Since the TargetScan database lacks data from Atlantogenata, we could only compare late-branching Boreoeutheria with a marsupial (opossum). Based on the number of conserved 3'-UTR sites (TargetScan database) of genes targeted by conserved microRNAs (MirGeneDB), *i.e.* those sites most likely to have been maintained by natural selection, we evaluated the following model to predict the cellular energy saving from the total number of conserved microRNA-target interactions per cell:

ΔTranslation cost = Median Sensitivity to Repression x Sites/Cell x AA Cost/Site

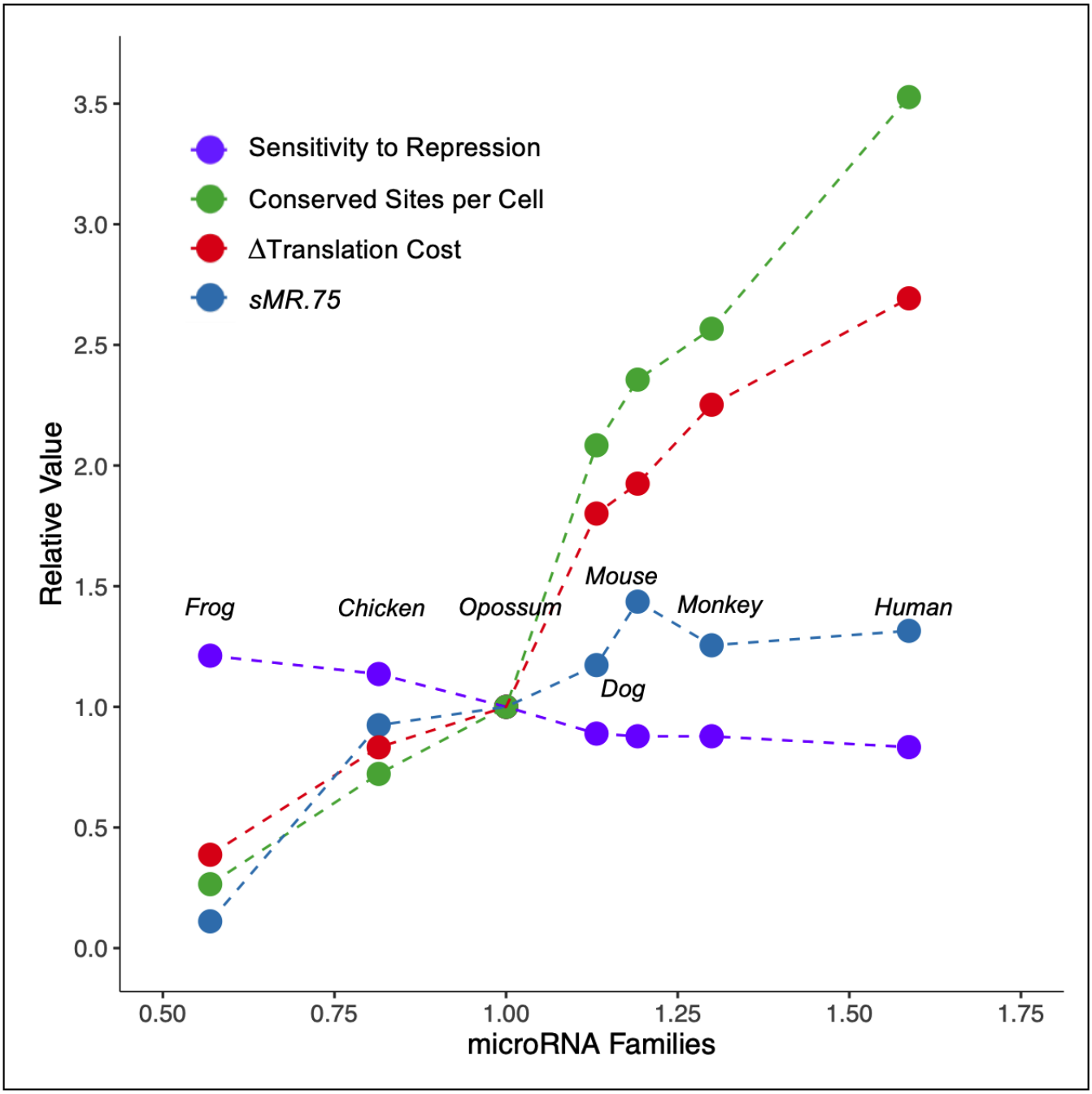

Figure 9. Evolution of factors in a model for energy cost saving by global microRNA activity.

Given that the cost of protein synthesis accounts for 18% of cellular metablic rate, we predicted that the ~ 30% increase in *sMR.75* between marsupials and late-branching placental mammals would be associated with an increase in overall microRNA-mediated repression of translation of ~ 167%. Figure 9 depicts the ratios of the value for each factor in the model to the corresponding value in the opossum. Relative to the opossum, the proportion of coding genes targeted and the number of 3'-UTR sites/mRNA were both approximately 50% higher in the placental mammals (Supplementary Tables 7). The total number of predicted microRNA-target site interactions per cell increased 100%, 140% and 250% in dog, mouse and human while the corresponding median values for sensitivity to repression by

combinatorial microRNA activity (C_n) decreased by 11%, 12% and 16.7% (Figure 9). After taking into account the distribution of target proteins 500 - 5,000 AA in length, the predicted differences in overall translation cost were 180%, 192% and 269% (Figure 9). Since the C_n values (combinatorial repression strengths) are based on the most effective microRNA from each family and likely to be overestimates (Agarwal et al, 2015; McGeary et al, 2019), these results are in reasonable agreement with our prediction.

DISCUSSION

Variable allometric scaling: a new method to explore the evolution of cellular MR

Given the high metabolic cost of protein synthesis and its strict relationship to cell size (Ginzberg et al, 2018; Björklund, 2019), we used variable allometric scaling in conjunction with phylogenetic comparative methods to directly analyse the dependence of the rMR/M^{exp} ratio on the size of the microRNA repertoire, complementing separate analyses of the variation of log mass and log *rMR* (Venditti et al, 2011; Baker et al, 2015; Avaria-Llautureo et al, 2019; White et al, 2019). The greater resolution of the arithmetic range of *rMR* for fitting M^{exp}, and the method's robustness to variation in mass made it possible to detect differences in the surface area dependence of the *sMR-miRNA.Fam* relationship, even between small groups of animals. The method itself, fitting the distribution of the rMR/M^{exp} ratio to that of third relevant trait, simulates a process of selection.

MirGeneDB is a new reference for comparative biology research.

Previous comparative studies have referenced molecular traits, such as genome size, the number of protein-coding genes, or quantity of non-coding DNA (for example, Choi et al, 2020). With the availability of the manually curated microRNA gene database, MirGeneDB, we are able to extend this approach to conserved microRNA families and genes in a wide range of vertebrate species and organs (Fromm et al, 2020; Fromm et al, 2021). A major concern in microRNA research in the past has been the quality of the online repository miRBase. This database contains many false-positives while at the same time missing a large number of *bona fide* microRNAs from undersampled species, which were misinterpreted as secondary losses (Chiang et al, 2010; Langenberger et al, 2011; Wang and Liu, 2011; Jones-Rhoades, 2012; Meng et al, 2012; Tarver et al, 2013; Castellano and Stebbing, 2013; Taylor et al, 2014; Fromm et al, 2015; Ludwig et al, 2017; Axtell et al, 2018; Fromm et al, 2020). Consequently, the conservation and utility of microRNAs as phylogenetic markers was questioned in the past (Thompson et al, 2014). However, these omissions were clearly technical artifacts, since losses of microRNA families have rarely been observed in well-annotated repertoires (Tarver et al, 2018). We and others have recently successfully employed MirGeneDB complements in a range of comparative (Fromm et al, 2021; Hu et al, 2021), phylogenetic (Ma et al, 2021; Rosani et al, 2021), developmental (Taylor et al, 2023; Jenike et al, 2023) and evolutionary studies (Peterson et al, 2022; Zolotarov et al,

2022), as a validation cohort for experimental findings (Kang et al, 2021; Baronti et al, 2020), and as a reference for the development of novel bioinformatics tools (https://github.com/sinanugur/MirMachine).

Exhaustive sequencing and genome curation have revealed that the number of families of conserved, microRNA-encoding genes has grown steadily over the course of vertebrate evolution, with very low rates of loss (Fromm et al, 2015; Tarver et al, 2018; Fromm et al, 2020; Fromm et al, 2021). Notably, the acquisition of shared microRNA families (Fromm et al, 2020) and conserved 3'-UTR target sites (Agarwal et al, 2015) accelerated in placental mammals, doubling the potential number of conserved microRNA-target interactions (Supplementary Tables S7). The acquisition of microRNA families and targets coincided closely with an elevation in *rMR*, body temperature and propensity for homeothermy among those mammalian orders that diverged more recently than Chiroptera (Ruf and Geiser, 2015; McNab, 2019): out of six mammalian orders with mean body temperatures significantly higher than that of bats, the only clade that diverged earlier than Chiroptera, Macroscelidea (Supplementary Figure S6), was a lineage characterized by an extreme reduction in size (Pagel et al, 2022). Conversely, out of eight orders with lower average body temperatures, the only one that diverged later than Chiroptera, Pholidota, is characterized by species with relatively large masses, low *MR*s and body temperatures near to ambient (Clarke et al, 2010; Supplementary Figure S6), indicative of a limited capacity to dissipate heat (Speakman and Król, 2010). Since the order Pholidota has undergone relatively few speciation events since the Cretaceous (Foley et al, 2023), this observation is a reminder that faster mechanisms of heat dissipation must have had to evolve hand in hand with faster rates of metabolic heat generation (Speakman and Król, 2010: Naya et al, 2013b; Fristoe et al, 2015).

Cellular MR variation with respect to miRNA.Fam fits a model of stabilizing selection

For a BM process, between-species trait covariances are proportional to their shared ancestry, and a BM model will be favored if most of the crown species diverged recently relative to the total age represented by the phylogeny, as in the case of the mammalian tree used in this study (Álvarez-Carretero et al, 2022). Furthermore, for a small sample and phylogeny the mvSLOUCH algorithm for the comparison of OU and BM models exhibits a bias towards BM that has been attributed to a difference in the effective population size for each process (Bartoszek, 2016). For example, in a reanalysis of Darwin's data for 13 species of finch (Harmon et al, 2008), two different measures of effective population size yielded correction factors of ~ 0.5 and ~ 0.9 for the BM and OU models, respectively (Bartoszek, 2016). However, even before applying an empirical correction for bias, we found that an OU process was consistently favored over a BM process as a model for the evolution of *sMR* with respect to *miRNA.Fam*, in both the 14-tetrapod and 10-mammal datasets.

Assuming constant rates of evolution, the optimal slopes obtained by phylogenetic linear regression for the dependence of *sMR* on *miRNA.Fam* across tetrapods or mammals were $M^{0.68}$ and $M^{0.71}$,

respectively (Supplementary Table S2). However, the AICc information criteria for both BM and OU models reached their minimal values when *sMR* was scaled to $M^{0.75}$, where BM and OU processes most precisely simulated the biphasic evolution of *sMR* (Supplementary Figure S5). This example illustrates an aspect of the scaling of *MR* that is generally overlooked when comparing allometric exponents obtained by the power law method, namely that differences in allometric slopes generally represent shifts in the rank order of the ratios between *sMR* and a third covariate. For example, in the sample of 10 mammals included in this study, the dog has the highest ratio of *sMR*/*miRNA.Fam* when *sMR* is scaled to $M^{0.70}$, third highest at $M^{0.75}$ and fourth lowest at $M^{0.80}$.

Three-quarter power scaling corresponds closely to the conserved slope of log *rMR*/log mass reported for mammals in countless reports since Kleiber (1932) and Brody and Proctor (1932) (see Introduction for additional references). Three-quarter power scaling of the OU model for the rate at which the *sMR* distribution converges towards that of the microRNA complement suggests that the relationship evolved under constraints similar to those governing the highly conserved ¾ power allometry between *MR* and mass, and supports the assumption that *miRNA.Fam* is a useful proxy for global microRNA activity. Furthermore, the concurrent increases in the branch-wise rates of evolution of *sMR*, *miRNA.Fam* and T_b support the notion that these relationships have been maintained by selection, and thus represent manifestations of a multivariate selection on *rMR* and *M* (White et al, 2019).

Analogous models with respect to microRNA genes exhibited the same $M^{0.75}$ optimum and a similar rate of adaptation for the OU process, but no optimum was observed for *sMR* variation in relation to genome size or the number of coding genes (Supplementary Figure S5). Thus, *sMR* variation appears to be specifically linked to the number of microRNA families. Since the mechanism by which microRNAs conserve metabolic energy is well established, the association with *sMR.75* presumably reflects the metabolic impact of global microRNA activity.

Optimally scaled MRs may also predict the microRNA complement in birds

In linear phylogenetic regressions, the optimal *sMR* scaling with respect to *miRNA.Fam* in tetrapods ($M^{0.68}$), mammals ($M^{0.71}$) and Boreoeutheria ($M^{0.70}$) exhibited greater dependence on surface area than did the log-based dependence of *rMR* on mass ($M^{0.78}$, $M^{0.77}$ and $M^{0.74}$, respectively). These shifts are reminiscent of the surface area dependence of field metabolic rates in mammals ($M^{0.68}$) and birds ($M^{0.58}$), in fair agreement with a model for the maximal rate of heat dissipation (Speakman and Króll, 2010). These observations may shed light on the correlation between vertebrate morphological patterns and microRNA complement size reported by Deline et al (2018). These authors demonstrated that morphological types were significantly related to the number of microRNA families, but not to genome size or the diversity of protein domains. Furthermore, the morphospace occupied by birds was significantly displaced from a reptilian-mammalian axis (Deline et al, 2018), an interesting parallel to the

shift we have predicted in birds, where *sMR*s are positively related to *miRNA.Fam* only when the allometric exponent is set lower than the ~ ⅔, *i.e.* slope of log *rMR*/log *M* (White et al, 2006; Fristoe et al, 2015; Ballesteros et al, 2018).

Furthermore, there is an important difference between birds and mammals in the regulatory context in which microRNAs operate. Ancestral birds underwent a reduction in genome size, from *c.* 2 Gb to *c.* 1 Gb, primarily by jettisoning transposable elements (TEs). The massive loss of TEs in the ancestral avian genome contrasts with the steady evolutionary accumulation of TEs in mammals, where, with the exception of bats, they occupy 40 - 50% of the genome (Zhang et al, 2014a; Kapusta et al, 2017; Platt et al, 2018). Retrotransposon sequences have been identified in the 3'- UTRs of 25% of mammalian coding genes and serve as binding sites for inhibitory KRAB-ZnF transcription factors (Faulkner et al, 2009). The loss of TEs in the ancestral bird genome was accompanied by the nearly complete loss of KRAB-ZnFs (Liu et al, 2014; Imbeault et al, 2017), implicating microRNA activity as the principal mechanism for the downregulation of gene expression in birds.

Interestingly, bat genomes are also characterized by smaller size, loss of transposable elements (Kapusta et al, 2017; Jebb et al, 2020) and shorter introns (Zhang and Edwards, 2012) relative to non-volant placental mammals, suggesting that these reductions represent adaptations for the faster rates of energy expenditure and signaling associated with flight (Hughes et al, 1995; Andrews et al, 2009; Wright et al, 2014; Ji and DeWoody, 2017). For example, shorter introns enable faster mRNA splicing (Heyn et al, 2014), while compact genomes and nuclei, if found in cells of smaller size and higher ratio of surface area/mass, would allow more rapid exchange of nutrients, as well as a higher density of neurons in the brain (Olkowicz et al, 2016; Gregory, 2018).

The predicted energy saved by global microRNA activity increased faster than cellular metabolic rate in placental mammals

The classification of conserved microRNA genes in MirGeneDB is congruent with the classification of conserved 3'-UTR target sites in TargetScan database (Kitai et al, 2022), but the latter lists targets for microRNAs that are excluded from the reference database, MirGeneDB. For example, of the 265 thousand sites listed for the human in the conserved site database, only 173 thousand corresponded to the reference microRNAs listed in MirGeneDB (Supplementary Tables S7). In order to exclude false positives, we considered only the targets of reference conserved microRNA families (see Methods).

For each species C_n, the cumulative combinatorial repression per site, was estimated from the median value of the distribution of "cumulative weighted context++ scores" (Agarwal et al, 2015). The CWCS model in the current version of TargetScan (.v8) accounts for 37% of the variation in messenger RNA levels following microRNA transfection of Hela cells, and probably overestimates the repression, since

for each site, only the interaction with the most effective member of a microRNA family is evaluated (McGeary et al, 2019).

After controlling for the number of coding genes in each species, and the distributions of the lengths of the targeted proteins, the estimated energy cost saved by global microRNA activity in placental mammals was double that found in the opossum, consistent with the ⅓ increase in s*MR*.75. Thus, even though the majority of mammalian-specific target sites appear to be evolving neutrally (Simkin et al, 2020), an increase in the overall number of such interactions may have provided an immediate energy-saving benefit.

An adaptive shift at the divergence of Boreoeutheria simulates the evolution of sMR

The advent of placentation allowed some orders to exploit high quality resources through an increase in energy expenditure and reproductive output, adaptations denied to monotremes and marsupials with access to the same resources (McNab, 2008). Among Boreoeutheria some clades, like Eulipotyphla and Chiroptera, retained the lower body temperatures (≤ 36°C) characteristic of early-branching placentals (Xenarthra and Afrotheria), while others evolved higher T_b's, such as Carnivora, Artiodactyla, primates and most rodents (Supplementary Figure S6). This divergence in body temperature regimes was associated with differences in the relative prevalence of homeothermy *versus* heterothermy *i.e.* daily torpor. Heterothermy is achieved by lowering the T_b set point, and evolved as an energy-saving strategy in small (< 1 kg) birds and mammals, notably bats, that are reliant on foraging and vulnerable to changes in food supply (Ruf and Geiser, 2015; Fjelldahl et al, 2022). After accounting for mass, climate and geography, early-branching orders exhibit more variable T_b (Boyles et al, 2013), a higher incidence of heterothermy (Ruf and Geiser, 2015), a lower proportion of skeletal muscle mass, and lower metabolic rates (McNab, 2019), compared to the majority of placental orders that diverged after Chiroptera where, as in birds, T_b > 36°C and permanent homeothermy predominate .

Our demonstration that the *sMR* distribution in mammals was best simulated by an adaptive shift at the divergence of Boreoeutheria, and its implication of a Simpsonian jump (Simpson, 1944), suggests a model with distinct adaptive optima for low- and high-T_b mammals, based on the present range of species in MirGeneDB (Fromm et al, 2021). Figure 10 illustrates estimated temperature gradients and optimal allometric exponents for the *sMR-miRNA.Fam* relationship based on five early-branching, low T_b mammals (including Atlanogenata) and five later-branching, high T_b mammals (Boroeuetheria) (Supplementary Table S2). A separate optimum is shown for birds, with a predicted allometric exponent shifted to below the allometric slope (0.64) of log *rMR*/log mass (Fristoe et al, 2015). The estimated temperature gradients maintained by the low- and high-T_b mammals differ by 8°C, correponding to a theoretical difference of 2.5% in thermodynamic efficiency, and potentially offsetting some of the cost of sustaining higher body temperatures (see Methods for data sources).

The inference of distinct adaptive peaks is based on the present range of mammalian microRNA repertoires in MirGeneDB, which represents only two of the four possible combinations of ancestry and phenotype: earlier-branching mammals with low T_b's and later-branching mammals with high T_b's.

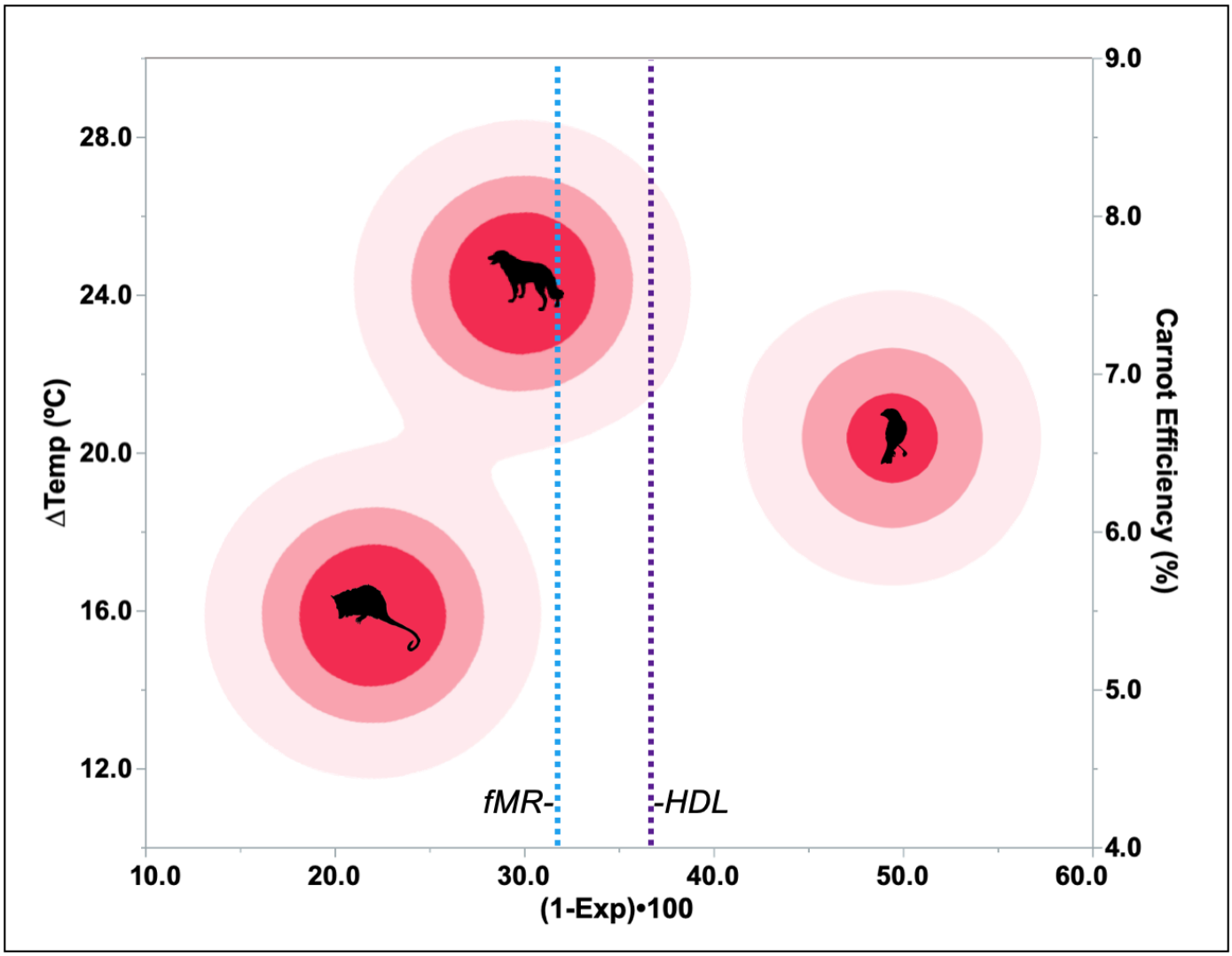

Figure 10. Contour plot of a hypothetical fitness landscape mapped onto the relationship beween the core-surface temperature gradient and the optimal allometric exponent of the *sMR-miRNA.Fam* relationship (see Methods for sources).
E_{opt} **:** Optimal *sMR-miRNA.Fam* scaling exponent. **ΔTemp =** Body temperature - Ambient temperature.
The dashed lines represent the allometric scaling of field metabolic rates and the predicted allometric scaling of the heat dissipation limit in mammals (Speakman and Król, 2010).
Silhouettes represent late-branching mammals (Boreoeutheria), earlier-branching mammals, and birds. (Phylophic © 2023: Marsupial, Sarah Werning; Dog, Tracy A. Heath; Bird, T. Michael Keesey).

The addition of definitive microRNA repertoires to intermediate branches of the mammalian tree, such as those of low T_b Eulipotyphla and Chiroptera, may eventually bridge these hypothetical optima, include examples of decreases in body temperature and uncoupling from the rate of evolution of metabolic rate (Avaria-Llautureo et al, 2019), and better conform to a gradual model of genetic drift (Pagel et al, 2022).

On the other hand, the evolution of T_b across 554 mammals has been found to be relatively static when compared to the rates of change of *MR* and ambient temperature (Avaria-Llautureo et al, 2019), consistent with an adaptive barrier to the emergence of higher body temperatures. As mammals diversified in size (thus ratio of surface area to mass) in response to cooler environments (Clavel and Morlon, 2017; Baker et al, 2015; Avaria-Llautureo, 2019), multiple anatomic and physiological mechanisms were available to adjust overall *MR* without altering T_b or cellular *MR*, including changes in thermal conductance (Naya et al, 2013b; Fristoe et al, 2015) and relative organ size (Wang et al, 2012), particularly that of skeletal muscle (Rowland et al, 2015; McNab, 2019; Wright et al, 2021). However, shifting to a higher T_b and cellular *MR* while maintaining the strict relationship between cell size and rate of protein synthesis during the cell cycle would have depended on the ability to synchronize the expression of hundreds of regulatory genes with the activities of their target pathways. Just such a role has been proposed for microRNAs: microRNA activity was essential to buffer the effect of temperature fluctuation on photoreceptor development in Drosophila (Li et al, 2009). When fruit fly larvae were genetically engineered to decrease *MR*, doubling the time to eclosion, the entire microRNA repertoire was rendered dispensable for normal development. According to the mechanism proposed by Cassidy et al (2019), the effectiveness of transient signalling by a transcription factors depends on the timely decay of its concentration. Since this decay rate is inversely related to the rate of protein synthesis, as metabolic rate increases, greater repressor activity is required to maintain the same, evolutionarily conserved, rate of decay. By analogy, increased repression by microRNAs may have been necessary to maintain the orderly unfolding of developmental programs in warmer, late-branching mammals. Bats are mammals that alternate between activity with thermoregulation to maintain homeoothermy or torpor, a state in which they are essentially ectotherms (Fjelldahl et al, 2022). According to the mechanism proposed above, the timing of transient signaling that is microRNA-dependent during homeothermy would be disrupted in the transition to torpor unless there were a temperature-related decrease in the rate of Ago2-loading, which is normally rate-limiting for global microRNA activity (Gebert and MacRae, 2019; Reichhof et al, 2019).

The majority of studies on the evolution of mammalian endothermy have focused on adaptations for the generation, conservation and dissipation of heat (*e.g.* Rowland et al, 2015; Legendre and Davesne, 2020), rather than on the mechanism of thermostatic control (Bernhardt et al, 2020). In this context, the emergence of permanent homeothermy among later-branching mammals can be understood as the endpoint of the evolution of the regulation of body temperature and the ultimate safeguarding of development from external perturbations, thereby allowing a more forward-looking and efficient allocation of energy among somatic maintenance, reproductive reserves, and parental care (Koteja, 2000; Maino et al, 2014; Swanson et al, 2017; Bernhardt et al, 2020). Our analysis of the relationships among *sMR*, *miRNA.Fam* and T_b in mammals has yielded evidence consistent with multivariate selection for stable and efficient thermoregulation. First, relative to mass, these three traits exhibited 7-

to 10-fold increases in evolutionary rate between the divergence of Atlantogenata and Boreoeutheria, independent of variation in mass. An increase above the background rate of evolution of 2-fold or more is considered evidence of positive phenotypic selection (Baker et al, 2016).

Second, Speakman and Król (2010) have argued that evolutionary fitness must depend more on field metabolic rate (*fMR*), *i.e.* the realized rate of energy expenditure over a period of days, than on basal metabolic rate (*bMR*), and proposed that *fMR* serve as the basis for testing their theory that variation in metabolic rate has been primarily constrained by the physiological limit on heat dissipation. Their phylogenetically-corrected allometric exponents for *fMR*s in mammals (0.68) and birds (0.58) agreed reasonably well with the slope of 0.63 predicted by their biophysical model of the maximal rate of heat dissipation (Speakman and Król (2010) (see Figure 10). There is additional biogeographic and physiological evidence for the theory that the maximal rate of heat dissipation and risk of hyperthermia have exerted a hard constraint on the upper end of variation in body temperature and metabolic rate.

Phylogenetically-informed patterns of geographic distribution indicate that the diversification of mammalian morphology has been asymmetric, with sizes increasing in most orders (Baker et al, 2015), but evolving more rapidly at higher latitudes and during cooler geologic eras (Clavel and Morlon, 2017). In a complementary fashion, the diversification of the limits of tolerance to cold temperatures evolved faster than the limits of tolerance to heat (Araújo et al, 2013; Cooney et al, 2016; Qu and Wiens, 2020), and fit a biased OU model, *i.e.* stronger selection on upper temperature limits (Bennett et al, 2021). To some extent the asymmetry may reflect a smaller range of habitat variation in warm climatic niches together with more options for behavioral, as opposed to physiological adaptation, but additional evidence supports the operation of a hard physiological constraint on heat dissipation:

(i) The difference that mammals are able to maintain between body temperature and ambient temperature is anti-correlated with ambient temperature (Pie et al, 2021; Supplementary Figure S7).

(ii) After controlling for mass and phylogeny, the anti-correlation between basal metabolic rates and the upper limit of the thermoneutral zone (the temperature above which cooling mechanisms must be activated in order to prevent hyperthermia) was three times steeper than the anti-correlation with the lower temperature limit (below which cold-induced thermogenesis is activated) (Khaliq and Hof, 2018).

(iii) Relative to unselected lines, inbred lines of bank voles selected for higher *rMR*s under thermoneutral conditions exhibited elevated body temperatures at 34ºC, indicating a diminished capacity for effective thermoregulation and increased risk of hyperthermia (Stawski et al, 2017).

In the present study, sliding window analysis revealed that the shift in optimal *sMR* scaling relative to *miRNA.Fam* in later-branching Boreoeutheria was significantly correlated with body temperature. The finding that the optimal slope in Boreoeutheria approaches that of field metabolic rate (Figure 10) suggests that the dependence of *sMR* on *miRNA.Fam* has been conditioned by limits on the rate of

heat dissipation (Speakman and Król, 2010). In other words, as evolving clades of Boreoeutheria increased in size (Baker et al, 2015) and/or rate of heat generation (Porter and Kearney, 2009), they were forced to negotiate a trade-off between gains in power and thermodynamic efficiency (larger ΔT_{b-a}), on the one hand, and an increased risk of hyperthermia, on the other. Such a trade-off would be a sufficient explanation for the asymmetric distributions of the physiological variables C_{min} (thermal conductance) and U_{CT} (the upper limit of the thermoneutral zone) among Boreoeutheria (Figure 11).

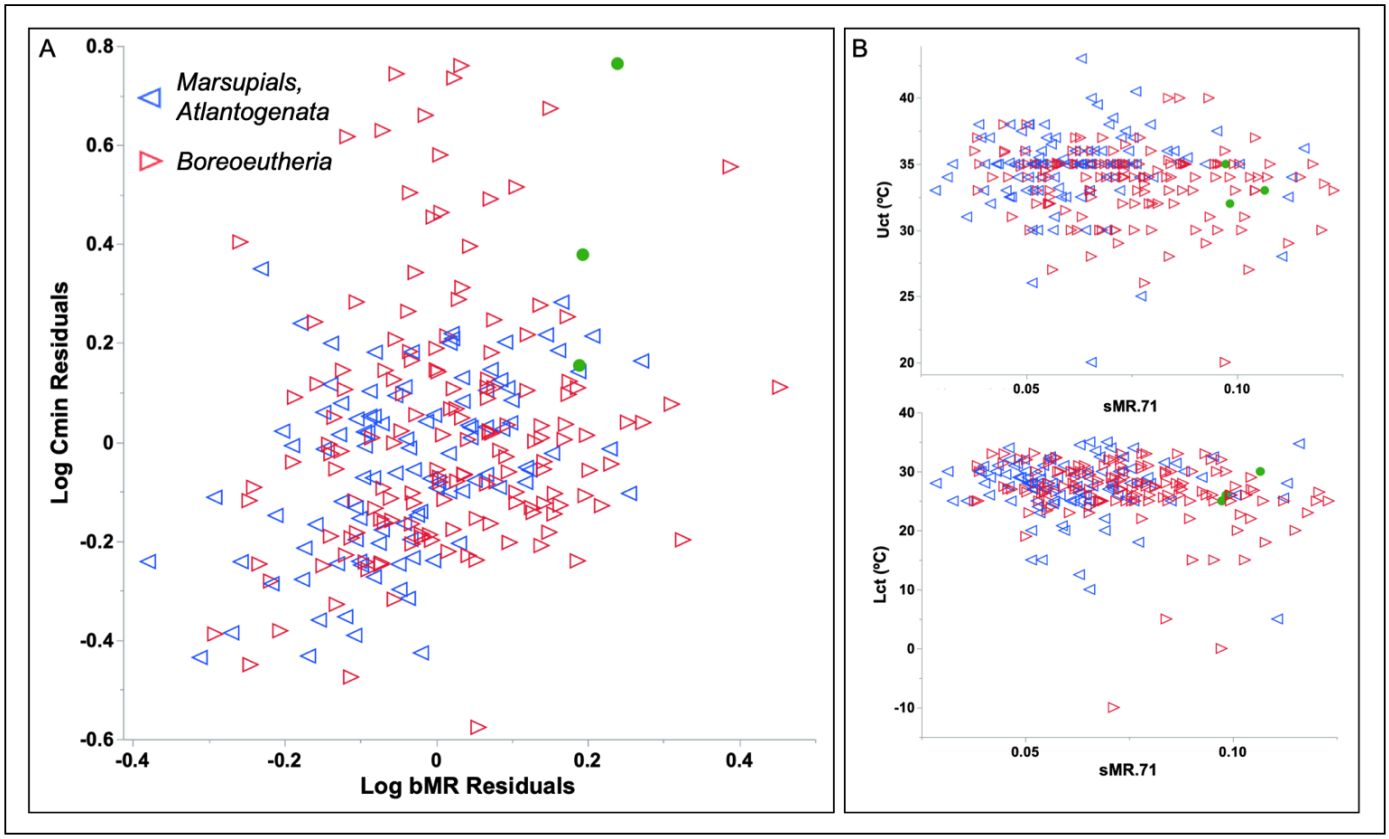

Figure 11. Shift in the distribution of Log C_{min} residuals, U_{CT} and L_{CT} among Boreoeutheria. The dataset (n = 242, including Chiroptera) was drawn from Khaliq et al (2014) (see Methods). U_{CT} and L_{CT} are plotted against *sMR* scaled optimally relative to *miRNA.Fam* across all mammals. Bovids are highlighted because of the well-known constraint that high ambient temperature imposes on the rate of lactation (for references, see Speakman and Król, 2010).

A comparison of the mass-independent residuals for C_{min} and *bMR* (Naya et al, 2013b; Fristoe et al, 2015) revealed that while the *bMR* residuals were evenly distributed between early- and late-branching mammals, the highest C_{min} residuals were found exclusively in Boreoeutheria (Figure 11A). In a complementary fashion, the distribution of both U_{CT} and L_{CT} among late-branching mammals were both shifted toward higher *sMR*s and lower temperatures, consistent with an asymmetric OU process that has 'pushed' diversification away from warmer niches and 'pulled' it toward cooler niches (Figure 11B)(Bennett et al, 2021).

The adaptive value of repression by individual microRNAs operating in gene regulatory networks has been attributed to their ability to canalize phenotypic expression by buffering the effects of environmental or allelic variation (Hornstein and Shomron, 2006; Li et al, 2009; Cassidy et al, 2013) and to set thresholds for cell fate determination (Mukherji et al, 2011; Ebert and Sharp, 2012). The ability of each microRNA seed to regulate many targets may have facilitated the evolution of regulatory networks of increasing complexity (Moran et al, 2017). Given the potential for microRNA regulation to increase the heritability of adaptive traits (Peterson et al, 2009), the enlargement of microRNA and target repertoires has been proposed as a key mechanism in the diversification of animal cell types and morphologies (Makeyev and Maniatis, 2008; Erwin et al, 2011; Deline et al, 2018; Dexheimer and Cochella, 2020; Peterson et al, 2021; Jenike et al, 2023; Taylor et al, 2023).

Relatively little attention has been paid to the nature of global microRNA activity (Reichholf et al, 2019; Kingston and Bartel, 2019; Tarbier et al, 2020; Kirstein et al, 2023) or its impact on energy metabolism (Schwanhäusser et al, 2011; Cassidy et al, 2019). Post-transcriptional regulation of gene expression ("mRNA processing") is the most constrained gene category in the evolutionary history of placental mammals (Christmas et al, 2023), which suggests a significant fitness cost for any loss in the efficiency of the processing of transcripts as mammals evolved faster and more complex regulatory networks. At the same time, the results of the present study indicate that the evolution in size of the microRNA-target apparatus has manifested an unexpected degree of integration with the cellular energy economy. Whatever the ultimate cause of the steady acquisition of microRNA families in vertebrates (Peterson et al, 2021), these observations are consistent with a role for global microRNA activity in maintaining metabolic efficiency and potentially facilitating an adaptive shift among late-branching placental mammals to higher body temperatures, faster metabolic rates, and permanent homeothermy.

DATA AVAILABILITY

The original data with accompanying references and the results of all analyses referred to in the text are provided in the Supplementary Information. Phylogenetic tree matrices are available upon request.

ACKNOWLEDGMENT

BF is supported by the Tromsø forskningsstiftelse (TFS) [20_SG_BF 'MIRevolution'].

AUTHOR CONTRIBUTIONS

Conceptualization: BF and TS; Methodology: TS; Investigation: BF and TS; Writing – Original Draft: TS; Writing – Review & Editing: BF and TS; Visualization: BF and TS; Funding Acquisition: BF.

DECLARATION OF INTERESTS

The authors declare no competing interests.

STAR METHODS

RESOURCE AVAILABILITY

LEAD CONTACT

For further information requests should be directed to Thomas Sorger (tsorger@rwu.edu).

MATERIALS AVAILABILITY

This study did not involve any physical material.

DATA AND CODE AVAILABILITY

The data compiled for this study are listed in Table S1 in the Supplementary Information.

All other data compilations are referenced in the main text.

This paper does not report original code.

METHOD DETAILS

MicroRNA Families, Genes and Targets

The numbers of conserved microRNA families and genes for 20 vertebrate species were obtained from MirGeneDB, a curated database of microRNA-encoding genes (Fromm et al, 2020). Conserved microRNAs were defined as those shared by two or more species. The number of conserved mammalian mRNA targets was extracted from the TargetScan8.0 database (Agarwal et al, 2015; McGeary et al, 2019) and filtered for targets corresponding only to conserved microRNAs.

Other Genomic Variables

Values for genome size and number of coding genes were obtained from the NCBI genome assembly database (as of March, 2022).

Body Temperatures and Ambient Temperatures

Body temperatures and ambient temperatures for mammals, excluding 20 multivariate outliers (mass, *bMR*) were obtained from Clarke et al (2010): differences of 24ºC and 16ºC were estimated for Boreoeutheria (n = 318) and earlier-branching mammals (n = 94). A gradient of 20ºC for birds < 1,200 g was estimated from mean body temperatures of 40ºC (n = 203; Fristoe et al 2015) and a mean ambient temperature of 20ºC, the average of maximum and minimum temperatures across the entire avian geographical distribution (n = 157; Khaliq et al, 2014). Mass-independent residuals for log Cmin, log *bMR*, and upper and lower critical temperatures were drawn from Khaliq et al (2015), after excluding multivariate outliers (mass, *bMR*) (n = 242).

QUANTIFICATION AND STATISTICAL ANALYSIS

Resting Metabolic Rates and Temperature Correction

Rates of oxygen consumption and body temperature were drawn primarily from the compilations of White et al (2006) and Gillooly et al (2017). Where multiple values had been recorded at different temperatures, we used the value nearest to the standard body temperature (see below). The original reference for each species is listed in Table S1 of the Supplementary Information. Resting metabolic rates (*rMR*s) were corrected to 38˚C for endotherms, and 25˚C for ectotherms, as *per* White et al (2006) and Gillooly et al (2017). Since oxygen consumption data were available only for *X. laevis*, and *X. tropicalis* adults are approximately half the size of adult *X. laevis*, we assumed 0.54 the *rMR* of *X. laevis* (assuming $rMR_2/rMR_1 = M_2^{0.88}/M_1^{0.88}$ for amphibia).

Phylogenies

"Phytools" was used to generate a 20-species vertebrate tree and phenogram, 14-species tetrapod tree and 10-species mammalian tree (Revell, 2012) based on divergence times drawn from Álvarez-Carretero et al (2022) for mammals, and Irisarri et al (2017) for earlier-branching vertebrates. Trees were made ultrametric and scaled to unit height using Mesquite © (2021).

In order to model the evolution of *miRNA.Fam*, a matrix of interspecific distances was assembled based on the number of conserved microRNA families (MirGeneDB: March, 2022) (Fromm et al, 2020), without considering losses or gains unique to each lineage. A distance tree was inferred by minimal evolution (LeFort et al, 2015).

Statistics

Phylogenetic linear regression was carried out using the *R: CAPER* package (Orme, 2013) using the maximum likelihood estimate between 0.0-1.0 for the *lambda* parameter (Pagel, 1999). All R^2 values were adjusted for the number of predictors.

Multivariate correlations, screening for outliers, ANCOVA and ordinal logistic regression were performed in JMP®16. For analysis of the fold variation by quintile in mass and cellular metabolic rate, Chiroptera and 21 outliers were removed from the original dataset of Clarke et al (2010). The cow was considered an outlier with respect to mass and, as in the case of all ruminants, metabolic rate (White and Seymour, 2005). All other statistical tests were performed in R (2020).

OU versus BM comparison and simulation

BM and OU models of the optimal *sMR* with respect to number of microRNA families were evaluated with the package mvSLOUCH (Bartoszek et al, 2012), with six repetitions of the hill-climbing algorithm for the OU process using two adaptation matrices (Diagonal and DecomposableReal). Preliminary

validation based on the AICc criterion revealed that for the 14 tetrapod model, OU processes were misclassified as BM for 50% of the simulations, while 10% of the BM simulations were misclassified as OU. The corresponding rates of misclassification for the 10 mammal model were 75% and 5% (n = 40, Supplementary Table S3). The rates of correct classification for the BM and OU simulations were equalized by adjusting the AICc scores +/- 2.1 for the tetrapod model, or +/- 4.0 for the mammalian model (Supplementary Table S3).

The Phylogenetic EM package (Bastide et al, 2018) was used to simulate *sMR* and *miRNA.Fam* distributions using variance/covariance matrix for *sMR.75* on *miRNA.Fam* as the selection strength matrix, with the median setting (3) for selection strength (Supplementary Figure S4). The average values for all mammals *sMR.75* and *miRNA.Fam* were assigned to the first adaptive shift (divergence of mammals), and the averages for all placentals were assigned to the second adaptive shift (divergence of Atlantogenata or Boreoeutheria or Euarchontoglires) (see Figure 5A). Ten simulations were generated and averaged for each shift or pair of shifts.

Bayesian inference of the branch-wise rates of evolution

For each individual trait, the VarRates algorithm of *BayesTraits* (version 4) was run for 12.5 million iterations with 20% burn-in and sampled every 1000 trees, yielding 10,000 trees fit to the distribution of either log mass, *sMR.75*, *miRNA.Fam* or T_b (Venditti et al, 2011). Bayes factors were obtained by comparing the 100 trees with the highest log likelihoods and the 100 trees with the smallest non-zero sum of scale changes. Correlations among the sets of branch lengths between the divergence of Theria and the divergence of Primates were obtained from the median branch lengths of the best 100 (1%) variable rate trees for each trait.

Variable Rate Regression and Inference of Internal Node Values

In order to evaluate the dependence of *sMR.75* on *miRNA.Fam*, while controlling for size (log mass) and body temperature, Bayesian regressions were run for 2.25 million iterations with 20% burn-in and sampled every 1000 trees (BayesTraits). Regression models using the 100/10,000 most likely variable rate trees for *sMR.75* were compared with models using the 100/10,000 trees with the smallest non-zero sum of scale changes.

Using the 11-mammal (including cow) variable rate tree for body temperature, and after optimizing the value (29°C) for the most recent common mammalian ancestor, body temperatures at the internal nodes were inferred from the directional variation model run for 8.0 million iterations with 20% burnin and sampled every 1000 trees.

Quantification of Model Interactions between Reference microRNAs and their 3'-UTR Target Sites

The entries in the TargetScan database "Conserved Site Context Scores" (Agarwal et al, 2015; McGeary et al, 2019) were filtered for the reference microRNAs listed for each species in MirGeneDB (Fromm et al, 2020). For each distribution of CWCS scores, the median value was used to estimate sensitivity to repression. In each species, a non-redundant list of target genes was used to compute the average number of 3'-UTR target sites/gene and the length distribution of the corresponding target proteins between 500 - 5,000 amino acids. The relative 'AA cost' was obtained from the weighted sum of nine 500 AA-length bins between 500 - 5,000 AA (Supplementary Table S7).

REFERENCES

Agarwal V, Bell GW, Nam J, Bartel DP. 2015. Predicting effective microRNA target sites in mammalian mRNAs. *eLife* 4: e05005.

Álvarez-Carretero S, Tamuri A, Battini M, Nascimento F, Carlisle E, Asher R, Yang Z, Donoghue P and Dos Reis M. 2022. A species-level timeline of mammal evolution integrating phylogenomic data. *Nature* 602: 263-267.

Andrews CB, Mackenzie SA and Gregory TR. 2009. Genome size and wing parameters in passerine birds. *Proc Roy Soc B* 276: 55-61.

Araújo MB, Ferri-Yáñez F, Bozinovic F, Marquet PA, Valladeres F and Chown SL. 2013. Heat freezes niche evolution. *Ecol Letters* doi: 10.1111/ele.12155 (1-14).

Avaria-Llautureo J, Hernandez CE, Rodriguez-Serrano E and Venditti, C. 2019. The decoupled nature of basal metabolic rate and body temperature in endotherm evolution. *Natur*e 572: 651-654.

Axtell MJ and Meyers BC. 2018. Revisiting criteria for plant microRNA annotation in the era of big data. *Plant Cell* 30: 272-284.

Baek D, Villén J, Shin C, Camargo FD, Gygi SP and Bartel DP. 2008. The impact of microRNAs on protein output. *Nature* 455: 64-72.

Baker J, Meade A, Pagel M and Venditti C. 2015. Adaptive evolution toward larger size in mammals. *PNAS* 112: 5093-5098.

Baker J, Meade A, Pagel M and Venditti C. 2016. Positive phenotypic selection inferred from phylogenies. *Biol J Linnean Soc* 118: 915-115.

Ballesteros FJ, Martinez VJ, Luque B, Lacasa L, Valor E and Moya A. 2018. On the thermodynamic origin of metabolic scaling. *Scientific Reports* 8: 1448.

Banerjee K, Kolomeisky AB and Igoshin OA. 2017. Elucidating interplay of speed and accuracy in biological error correction. *PNAS* 114: 5183-5188.

Barato AC and Seifert U. 2015. Thermodynamic uncertainty relation for biomolecular processes. *Phys Rev Lett* 114: 158101.

Baronti L, Guzzetti I, Ebrahimi P, Sandoz SF, Steiner E, Schlagwitneit J, Fromm B, Silva L, Fontana C, Chen AA and Petzold K. 2020. Base-pair conformational switch modulates miR-34a targeting of Sirt1 mRNA. *Nature* 583: 139-144.

Bartel DP. 2018. Metazoan MicroRNAS. *Cell* 173: 20-51.

Bartel DP and Chen CZ. 2004. Micromanagers of gene expression: the potentially widespread influence of metazoan microRNAs. *Nature Genet* 5: 396-400.

Bartoszek K. 2016. Phylogenetic effective sample size. *J Theor Biol* 4017: 371-386.

Bartoszek K, Pienaar J, Mostad P, Andersson S and Hansen TF. 2012. A phylogenetic comparative method for studying multivariate adaptation. *J Theor Biol* 314: 204-215.

Bastide P, Mariadassou M and Robin S. 2018. Detection of adaptive shifts on phylogenies by using shifted stochastic processes on a tree. *J R Stat Soc B 79*: 1067-1093.

Bennett CH. 1979. Dissipation-error tradeoff in proofreading. *Biosystems* 11: 85-91.

Bennett JM, Sunday J, Calosi P, Villalobos F, Martínez B, Molina-Venegas R, Araújo MB, Algar AC, Clusella-Trulas S, Hawkins BA, Keith SA, Kühn I, Rahbek C, Rodríguez L, Singer A, Morales-Castilla I and Olalla-Tárraga MA. 2021. The evolution of critical thermal limits of life on Earth.
Nature Comms 12: 1198 (1-9).

Benson RBJ, Godoy P, Bronzati M, Butler RJ and Gearty W. 2022. Reconstructed evolutionary patterns for crocodile-line archosaurs demonstrate impact of failure to log-transform body size data. *Communications Biology* 171: 1-4.

Bernhardt JR, O'Connor MI, Sunday JM and Gonzalez A. 2020. Live in fluctuating environments.
Phil Trans R Soc B 375: 20190454 (1-22).

Björklund M. 2019. Cell size homeostasis: Metabolic control of growth and cell division.
BBA Mol Cell Res 1866: 409-417.

Boyles JG, Thompson AB, McKechnie AE, Malan E, Humphries MM and Careau. 2013.
A global heterothermic continuum in mammals. *Global Ecol Biogeogr* 22: 1029-1039.

Brody S and Proctor RC. 1932. Relation between basal metabolism and mature body weight in different species of mammals and birds. *Univ Missouri Agr Exp Stn Res Bull* 166: 89–101.

Buttgereit F and Brand MD. 1995. A hierarchy of ATP-consuming processes in mammalian cells. *Biochem J* 312: 163-167.

Cassidy JJ, Bernasek SM, Bakker R, Giri R, Peláez, N, Eder B, Bobrowska A, Bagheri N, Amaral LAN and Carthew RW. 2019. Repressive gene regulation synchronizes development with cellular metabolism. *Cell* 178: 1-13.

Cassidy JJ, Jha JR, Posadas DM, Giri R, Venken KJT, Ji J, Jiang H, Bellen HJ, White KP and Carthew RW. 2013. miR-9a Minimizes the Phenotypic Impact of Genomic Diversity by Buffering a Transcription Factor. *Cell* 155: 1556-1567.

Castellano L and Stebbing J. 2013. Deep sequencing of small RNAs identifies canonical and non-canonical microRNA and endogenous siRNAs in mammalian somatic tissues.
Nucl Acid Res 41: 3339-3351.

Chiang HR, Schoenfeld LW, Ruby JG, Auyeung VC, Spies N, Baek D, Johnston WK, Russ C, Luo S, Babiarz JE et al. 2010. Mammalian microRNAs: experimental evaluation of novel and previously annotated genes. *Genes Dev* 24: 992-1009.

Choi IY, Kwon EC and Kim NS. 2020. The C- and G-value paradox with polyploidy, repeatomes, introns, phenomes and cell economy. *Genes Genomics*: 699-714.

Christmas MJ, Kaplow IM, Genereux DP and many others. 2023. Evolutionary constraint and innovation across hundreds of placental mammals. *Science* 380: eabn3943 (1-15).

Clarke A, Rothery P and Isaac NJP. 2010. Scaling of basal metabolic rate with body mass and temperature in mammals. *J Animal Ecol* 79: 610-619.

Clavel J and Morlon H. 2017. Accelerated body size evolution during cold climatic periods in the Cenozoic. *PNAS* 114: 4183-4188.

Cooney CR, Seddon N and Tobias JA. 2016. Widespread correlations between climatic niche evolution and species diversification in birds. *J Animal Ecol* 85: 869-878.

Deline B, Greenwood JM, Clark JW, Puttick MN, Peterson KJ, Donoghue PCJ. 2018. Evolution of metazoan morphological disparity. *PNAS* 29: E8909-E8918.

del Vecchio D, Dy AJ and Qian Y. 2016. Control theory meets synthetic biology.
J. R. Soc. Interface 13: 20160380 (1-17).

Dexheimer PJ and Cochella L. 2020. MicroRNAs: from mechanism to organism.
Frontiers in Cell and Dev Biol 8: 409.

Ebert MS and Sharp PA. 2012. Roles for MicroRNAs in conferring robustness to biological processes. *Cell* 149: 515-524.

Eisenberg E and Levanon E. 2003. Human housekeeping genes are compact.
Trends Genet 19: 362-365

Erwin DH, Laflamme M, Tweedt SM, Sperling EA, Pisani D and Peterson KJ. 2011. The Cambrian conundrum: early divergence and later ecological success in the early history of animals.
Science 334: 1091-1097.

Faulkner GF, Kimura Y, Daub CO, Wani S, Plessy C, Irvine KM, Schroder K et al. 2009. The regulated retrotransposon transcriptome of mammalian cells. *Nature Genet* 41: 563-571.

Felsenstein J. 1985. Phylogenies and the comparative method. *American Naturalist* 125: 1-15.

Fjelldal MA, Søras R and Stawski C. 2022. Universality of Torpor Expression in Bats.
Physiol Biochem Zool 95: 326-339.

Foley NM, Mason VC, Harris AJ, Bredemeyer KR, Damas J, Lewin HA, Eizirik E, Gatesy J, Karlsson EK, Lindblad-Toh K, Zoonomia Consortium, Springer MS and Murphy WJ. 2023. A genomic timescale for placental mammal evolution. Science 380: eabl8189 (1-9).

Friedman RC, Farh KKH, Burge CB and Bartel DP. 2009. Most mammalian mRNAs are targets of microRNAs. *Genome Res* 19: 92-105.

Fristoe TS, Burger JR, Balk MA, Khaliq I, Hof C and Brown JH. 2015. Metabolic heat production and thermal conductance are mass-independent adaptations to the thermal environment in birds and mammals. *PNAS* 112: 15934-15939.

Fromm B, Billipp T, Peck LE, Johansen M, Tarver JE, King BL, Newcomb JM, Sempere LF, Flatmark K, Hovig E and Peterson KJ. 2015. A uniform system for the annotation of vertebrate microRNA genes and the evolution of the human microRNAome. *Ann Rev Genet* 49: 213-242.

Fromm N, Domanska F, Høye F, Ovchinnikov V, Kang E, Aparicio-Puerta R, Johansen M, Flatmark K, Mathelier A, Hovig E, Hackenberg M, Friedländer MR and Peterson KJ. 2020. MirGeneDB 2.0: The metazoan microRNA complement. *Nucl Acids Res* 48: D132–D141.

Fromm B, Høye E, Domanska D, Zhong X, Aparicio-Puerta E, Ovchinnikov V, Umu SU, Chabot, PJ, Kang W, Aslanzadeh M, Tarbier M, Mármol-Sánchez E, Urgese G, Johansen M, Hovig E, Hackenberg M, Friedländer MR and Peterson KJ. 2021. MirGeneDB 2.1: toward a complete sampling of all major animal phyla. *Nucl Acids Res* 50: D204-D210.

Fromm B, Tarbier M, Smith O, Mármol-Sánchez E, Dalén L, Gilbert MTP and Friedländer MR. 2021. Ancient microRNA profiles of 14,300-yr-old canid samples confirm taxonomic origin and provide glimpses into tissue-specific gene regulation from the Pleistocene. *RNA* 27: 324-334.

Gebert LFR and MacRae IJ. 2019. Regulation of microRNA function in animals.
Nature Reviews Mol Cell Biol 20: 21-37.

Gillooly JF, Gomez JP and Mavrodiev EV. 2017. A broad-scale comparison of aerobic activity levels in vertebrates: endotherms versus ectotherms. *Proc R Soc B* 284: 20162328.

Ginzberg MB, Chang N, D'Souza H, Patel N, Kafri R and Kirschner MW. 2018. Cell size sensing in animal cells coordinates anabolic growth rates and cell cycle progression to maintain cell size uniformity. *elife* 7: e26957.

Gregory TR. 2018. Genome size and brain cell density in birds. Can J Zool 96: 379-382.

Harmon LJ, Weir JT, Brock CD, Glor RE and Challenger W. 2008. GEIGER: investigating evolutionary radiations. *Bioinformatics* 24: 129–131.

Heyn P, Kalinka AT, Tomancak P and Neugebauer KM. 2014. Introns and gene expression: Cellular constraints, transcriptional regulation, and evolutionary consequences. *Bioessays* 37: 148–154.

Hopfield JJ. 1974. Kinetic proofreading: A new mechanism for reducing errors in biosynthetic processes requiring high specificity. *PNAS* 71: 4135-4139.

Hornstein H and Shomron N. 2006. Canalization of development by microRNAS.
Nature Genetics 38: S20-S24.

Hu RS, Zhang XX, Ma QN, Elsheika HM, Ehsan M, Zhao Q, Fromm B and Zhu XQ. 2021. Differential expression of microRNAs and tRNA fragments mediate the adaptation of the liver fluke *Fasciola gigantica* to its intermediate snail and definitive mammalian hosts. *Int J Parasitol* 51: 405-414.

Hughes AL and Hughes MK. 1995. Small genomes for better flyers. *Nature* 377: 391.

Imbeault M, Helleboid PY and Trono D. 2017. KRAB zinc-finger proteins contribute to the evolution of gene regulatory networks. *Nature* 543: 550-554.

Irisarri I, Baurain D, Brinkmann H, Delsuc F, Sire JY, Kupfer A, Petersen J, Jarek M, Meyer A, Vences M, and Philippe H. 2017. Phylotranscriptomic consolidation of the jawed vertebrate timetree. *Nature Ecol Evol* 1: 1370-1378.

Jebb D, Huang Z, Pippel M, et al. 2020. Six reference-quality genomes reveal evolution of bat adaptations. *Nature* 583: 578–584.

Jenike AE, Jenike KM, Peterson KJ, Fromm B and Halushka MK. 2023. Direct observation of the evolution of cell-type-specific microRNA expression signatures supports the hematopoietic origin model of endothelial cells. *Evol Dev* 25: 226-239.

Ji Y and DeWoody JA. 2017. Relationships Among Powered Flight, Metabolic Rate, Body Mass, Genome Size, and the Retrotransposon Complement of Volant Birds. *Evol Biol* 44: 261–272.

Jones-Rhoades MW. 2012. Conservation and divergence in plant microRNAs. *Plant Mol Biol* 80: 3-16.

Kafri M, Metzi-Raz E, Jonas F and Barkai N. 2016. Rethinking cell growth models.
FEMS Yeast Research 16: fow081

Kang W, Fromm B, Houben AJ, Høye E, Bezdan D, Arnan C, Thrane K, Asp M, Johnson R, Biryukova I and Friedländer MR. 2021. MapToCleave: High-throughput profiling of microRNA biogenesis in living cells. *Cell Rep* 37: 110015.

Kapusta A, Suh A and Feschotte. 2017. Dynamics of genome size evolution in birds and mammals. *PNAS* 114: E1460-E1469.

Khaliq I, Hof C, Prinzinger R, Böhning-Gaese K and Pfenninger M. 2014. Global variation in thermal tolerances and vulnerability of endotherms to climate change. *Proc Roy Soc B* 281: 20141097 (1-8).

Khaliq I and Hof C. 2018. Testing the heat dissipation limitation hypothesis: basal metabolic rates of endotherms decrease with increasing upper and lower critical temperatures. *PeerJ* 6:e5725 (1-13).

Kingston ER and Bartel DP. 2019. Global analyses of the dynamics of mammalian microRNA metabolism. *Genome Res* 29: 1777-1790.

Kirstein N, Dokaneheifard S, Cingaram PR, Valencia MR, Beckedorff F, Dos Santos G, Blumenthal E, Tayari MM, Gaidosh GS and Shiekhattar R. 2023. The Integrator complex regulates microRNA abundance through RISC loading. *Sci Adv* 9: eadf0597 (1-17).

Kitai H, Ogami K, Komatsu S, Watanabe Y, Yoshino S, Koshi E, Tsubota S, Funahashi Y, Takahiro M, Furuhashi K, Ishimoto T, Kosugi T, Maruyama S, Kadumatsu K and Suzuki H. 2022. Systematic characterization of seed overlap microRNA cotargeting associated with lupus pathogenesis.
BMC Biol 20: 248 (1-23).

Kleiber M. 1932. Body size and metabolism. *Hilgardia* 6: 315-353.

Knapp BD, Odermatt P, Rojas ER, Cheng W, He X, Huang KC and Chang F. 2019. Decoupling of Rates of Protein Synthesis from Cell Expansion Leads to Supergrowth. *Cell Systems* 9: 434-445.

Koteja P. 2000. Energy assimilation, parental care and the evolution of endothermy.
Proc R Soc B. 267: 479-484.

Krek A, Grün D, Poy MN, Wolf R, Rosenberg L, Epstein EJ, MacMenamin P, de Piedade I, Gunsalus KC, Stoffel M and Rajewsky N. 2005. Combinatorial microRNA Predictions.
Nature Genetics 37: 495-500.

Langenberger D, Bartschat S, Hertel J, Hoffmann S, Tafer H and Stadler PF. 2011. MicroRNA or not microRNA? Advances in Bioinformatics and Computational Biology.
pp 1-9. Springer (Berlin, Heidelberg).

Lefort V, Desper R and Gascuel O. 2015. A comprehensive, accurate and fast distance-based phylogeny inference program. *Mol Biol Evol* 32: 2798-800.

Legendre LJ and Davesne D. 2020. The evolution of mechanisms involved in vertebrate endothermy. *Phil Trans R Soc B* 375: 20190136 (1-12).

Li X, Cassidy JJ, Reinke CA, Fischboeck S and Carthew RW. 2009. A microRNA imparts robustness against environmental fluctuation during development. *Cell* 137: 273-282.

Lin J and Amir A. 2018. Homeostasis of protein and mRNA concentrations in growing cells. *Nature Comm* 9: 4496.

Lin J and Amir A. 2021. Disentangling intrinsic and extrinsic gene expression noise in growing cells. *Phys Rev Lett* 126: 078101

Liu H, Chang LH, Sun Y, Lu X and Stubbs L. 2014. Deep vertebrate roots for mammalian zinc finger transcription families. *Genome Biol Evol* 6: 510-525.

Lu GA, Zhang J, Zhao Y, Chen Q, Lin P, Tang Z, Wen H, Liufu Z and Wu CI. 2023. Canalization of phenotypes—when the transcriptome is Constantly but weakly perturbed. *Mol Biol Evol* 40: msad005.

Ludwig N, Becker M, Schumann T, Speer T, Fehlmann T, Keller A and Meese B. 2017. Bias in recent miRBase annotations potentially associated with RNA quality issues. *Sci Rep* 7: 5162.

Lynch M and Marinov GK. 2015. The bioenergetic costs of a gene. *PNAS* 112: 15690-15695.

Ma X, He K, Shi Z, Li M, Li F and Chen XX. 2021. Large-Scale Annotation and Evolution Analysis of microRNA in Insects. *Genome Biol Evol* 13: evab083.

Maino JL, Kearney MR, Nisbet RM and Kooijman SALM. 2014. Reconciling theories for metabolic scaling. *J Animal Ecol* 83: 20-29.

Makeyev EV and Maniatis T. 2008. Multilevel Regulation of Gene Expression by MicroRNAs. *Science* 319: 1789-1790.

Mallory JD, Kolomeisky AB and Igoshin OA. 2019. Trade-offs between error, speed, noise, and energy dissipation in biological processes with proofreading. *J Phys Chem B* 123: 4718-4725.

McGeary SE, Lin KS, Shi CY, Pham TM, Bisaria N, Kelley GM and Bartel DP. 2019. The biochemical basis of microRNA targeting efficacy. *Science* 366: eaav1741.

McNab BK. 2008. An analysis of the factors that influence the level and scaling of mammalian BMR. *Comp Biochem Physiol A* 151, 5-28.

McNab BK. 2009. Ecological factors affect the level and scaling of avian BMR.
Comp Biochem Physiol A 152: 22-45.

McNab BK. 2019. What determines the basal rate of metabolism? *J Exp Biol* 222: jeb205591.

Meng Y, Shao C, Wang H and Chen M. 2012. Are all the miRBase-registered microRNAs true? A structure- and expression-based re-examination in plants. *RNA Biol* 9: 249-253.

Moran Y, Agron M, Praher D and Technau U. 2017. The evolutionary origin of plant and animal microRNAs. *Nature Ecol Evol* 1: 0027.

Mukherji S, Ebert MS, Zheng GXY, Tsang JS, Sharp PA and van Oudenaarden A. 2011. MicroRNAs can generate thresholds in target gene expression. *Nature Genetics* 43: 854-859.

Naya DE, Spangenberg L, Naya H and Bozinovic F. 2013a. How does evolutionary variation in metabolic rate arise? A statistical assessment and a mechanistic model. *Evolution* 67: 1463-1476.

Naya DE, Spangenberg L, Naya H and Bozinovic F. 2013b. Thermal conductance and basal metabolic rate are part of a coordinated system for heat transfer regulation. *Proc Roy Soc B* 280: 20131629 (1-7).

Neurohr GE, Terry RL, Lengefeld J et al. 2019. Excessive Cell Growth Causes Cytoplasm Dilution And Contributes to Senescence. *Cell* 176: 1083-1097.

Ninio J. 1975. Kinetic amplification of enzyme discrimination. *Biochimie* 57: 587-595.

Olkowicz S, Kocourek M, Lucan RK, Portes M, Fitch WT, Herculano-Houzel S and Nemec P. 2016.
Birds have primate-like numbers of neurons in the forebrain. *PNAS* 113: 7255–7260.

Orme D, Freckleton RP, Thomas GH and Petzoldt T. 2013. CAPER: comparative analyses of phylogenetics and evolution in R. *Methods Ecol and Evol* 3: 141-151.

Ozbudak EM, Thattai M, Kurtser I, Grossman AD and van Oudenaarden. 2002. Regulation of noise in the expression of a single gene. *Nature Genetics* 31: 69-73.

Pagel M. 1999. Inferring the historical patterns of biological evolution.
Nature 401: 877-884.

Pagel M, O'Donovan C and Meade A. 2022. General statistical model shows that macroevolutionary patterns and processes are consistent with Darwinian gradualism. *Nat Commun* 13, 1113.

Peterson KJ, Dietrich MR and McPeek, MA. 2009. MicroRNAs and metazoan macroevolution: insights into canalization, complexity, and the Cambrian explosion. *BioEssays* 31: 736–747.

Peterson KJ, Beavan A, Chabot PJ, McPeek MA, Pisani D, Fromm B and Simakov O. 2022. MicroRNAs as Indicators into the Causes and Consequences of Whole-Genome Duplication Events. *Mol Biol Evol* 39: msab344.

Peth A, Nathan JA and Goldberg AL. 2013. The ATP Costs and Time Required to Degrade Ubiquitinated Proteins by the 26 S Proteasome. *J Biol Chem* 288: 29215-29222.

Pie MR, Divieso R and Caron FS. 2021. The evolution of climatic niche breadth in terrestrial vertebrates. *J Zool Syst Evol Res* 59: 1155–1166.

Platt RN, Vandewege MW and Ray DA. 2018. Mammalian transposable elements and their impacts on genome evolution. *Chromosome Res* 26:25–43.

Porter WP and Kearney M. 2009. Size, shape, and the thermal niche of endotherms. 2009. *PNAS* 106: 19666–19672.

Qu YF and Wiens JJ. 2020. Higher temperatures lower rates of physiological and niche evolution. *Proc R. Soc B* 287: 0823 (1-10).

R Core Team. 2020. R: a language and environment for statistical computing. R Foundation for Statistical Computing. Vienna, Austria.

Raftery AE. 1996. Hypothesis testing and model selection. In: Gilks WR, Richardson S and Spiegelhalter DJ, eds. Markov Chain Monte Carlo in Practice. London, UK: Chapman & Hall, 163–187.

Reichholf B, Herzog VA, Fasching N, Manzenreither RA, Sowemimo I and Ameres, SL. 2019. Time-Resolved Small RNA Sequencing Unravels the Molecular Principles of MicroRNA Homeostasis. *Molecular Cell* 75: 756-768.

Revell LJ. 2010. Phylogenetic signal and linear regression on species data.
Methods Ecol Evol 1: 319-329.

Revell LJ. 2012. phytools: an R package for phylogenetic comparative biology (and other things). *Methods Ecol Evol* 3: 217–223.

Rolfe DF, and Brown GC. 1997. Cellular energy utilization and molecular origin of standard metabolic rate in mammals. *Physiol Rev* 77: 731-58.

Rosani U, Bortoletto E, Bai CM, Novoa B, Figueras A, Venier P and Fromm B. 2021. Digging into bivalve microRNAomes: between conservation and innovation. *Philos Trans R Soc B* 376:20200165.

Rowland LA, Bal NC, Periasamy M. 2015. The role of skeletal-muscle-based thermogenic mechanisms in vertebrate endothermy. *Biol Rev Camb Philos Soc* 90:1279-97.

Ruf T and Geiser F. 2015. Daily torpor and hibernation in birds and mammals. *Biol Reviews* 90: 891-926.

Savage, VM, Gillooly JF, Woodruff, WH, West GB, Allen AP, Enquist BJ and Brown AC. 2004. The predominance of quarter-power scaling in biology. *Funct Ecol* 18: 257–282.

Schmiedel JM, Klemm SL, Zheng Y, Sahay A, Blüthgen N, Marks DS and van Oudenaarden A. 2015. MicroRNA control of protein expression noise. *Science* 348: 128-132.

Schmiedel JM, Carey LB and Lehner B. 2019. Empirical mean-noise fitness landscapes reveal the fitness impact of gene expression noise. *Nature Comms* 10: 3180.

Scholander PF, Hock R, Walters V, Johnson F and Irving L. 1950. Heat regulation in some arctic and tropical mammals and birds. *Biol Bull* 99: 237-258.

Schwanhäusser B, Busse D, Li N, Dittmar G, Schuchhardt J, Wolf J, Chen W and Selbach M. 2011. Global quantification of mammalian gene expression control. *Nature* 473: 337–342.

Selbach M, Schwanhäusser B, Thierfelder N, Fang Z, Khanin R, Rajewsky N. 2008. Widespread changes in protein synthesis induced by microRNAs. *Nature* 455: 58–63.

Simkin A, Geissler R, McIntyre ABR, and Grimson A. 2020. Evolutionary dynamics of microRNA target sites across vertebrate evolution. *PLoS Genetics* 16: e1008285.

Simpson GG. 1944. Tempo and Mode in Evolution. Columbia University Press. New York.

Singh A. 2011. Negative feedback Through mRNA provides the best control of gene-expression noise. *IEEE Trans NanoBioscience* 10: 194-200.

Snoberger A, Anderson RT and Smith DM. 2017. The Proteasomal ATPases Use a Slow but Highly Processive Strategy to Unfold Proteins. *Front Mol Biosci* 4: 18 (1-9).

Speakman JR and Król E. 2010. Maximal heat dissipation capacity and hyperthermia risk: neglected key factors in the ecology of endotherms. *J Anim Ecol* 79: 726–746.

Spies N, Burge CB and Bartel DP. 2013. 3' UTR-isoform choice has limited influence on the stability and translational efficiency of most mRNAs in mouse fibroblasts. *Genome Res* 23: 2078-2090.

Stawksi C, Koteja P and Sadowska ET. 2017. A Shift in the Thermoregulatory Curve as a Result of Selection for High Activity-Related Aerobic Metabolism. *Front Physiol* 8: 1070 (1-11).

Swanson DL, McKechnie AE and Vézina F. 2017. How low can you go? An adaptive energetic framework for interpreting basal metabolic rate variation in endotherms.
J Comp Physiol B 187: 1039-1056.

Tarbier M, Mackowiak SD, Frade J, Catuara-Solarz S, Biryukova I, Gelali E, Menéndez DB, Zapata L, Ossowski S, Bienko M, Gallant CJ, and Friedländer MR. 2020. Nuclear gene proximity and protein interactions shape transcript covariations in mammalian single cells. *Nature Comms* 11: 5445 (1-11).

Tarver JE, dos Reis M, Mirarab S, Moran RJ, Parker S, O'Reilly JE, King BL, O'Connell MJ, Asher RJ, Warnow T, Peterson KJ, Donoghue PCJ and Pisani D. 2016. The Interrelationships of Placental Mammals and the Limits of Phylogenetic Inference. *Genome Biol Evol* 8: 330-344.

Tarver JE, Sperling EA, Nailor A, Heimberg AM, Robinson JM, King BL, Pisani D, Donoghue PCJ and Peterson KJ. 2013. microRNAs: Small Genes with Big Potential in Metazoan Phylogenetics.
Mol Biol Evol 30: 2369-2382.

Tarver JE, Taylor RS, Puttick MN, Lloyd GT, Pett W, Fromm B, Schirrmeister BE, Pisani D, Peterson KJ and Donoghue PCJ. 2018. Well-annotated microRNAomes do not evidence pervasive microRNA loss. *Genome Biol Evol* 10: 1457-1470.

Taylor AS, Tinning H, Ovchinnikov V, Edge J, Smith W, Pullinger AL, Sutton RA, Constantinides B, Wang D, Forbes K, Forde N and O'Connell MJ. 2023. A burst of genomic innovation at the origin of placental mammals mediated embryo implantation. *Comm Biol* 6:459 (1-8).

Taylor RS, Tarver JE, Hiscock SJ and Donoghue PC. 2014. Evolutionary history of plant microRNAs. *Trends Plant Sci* 19: 175-182.

Thattai M and van Oudenaarden A. 2001. Intrinsic noise in gene regulatory networks.
PNAS 98: 8614-8619.

Thompson RC, Plachetzki DC, Mahler DL, Moore BR. 2014. A critical appraisal of the use of microRNA data in phylogenetics. *PNAS* 111: E3659–3668.

Venditti C, Meade A and Pagel M. 2011. Multiple routes to mammalian diversity. *Nature* 479: 393-396.

Vogel C, Abreu R, Ko D, Le S, Shapiro BA, Burns SC, Sandhu D, Boutz DR, Marcotte EM and Penalva LO. 2010. Sequence signatures and mRNA concentration can explain two- thirds of protein abundance variation in a human cell line. *Mol Syst Biol* 6: 400.

Wagner A. 2005. Energy Constraints on the Evolution of Gene Expression.
Mol Biol Evol 22: 1365–1374.

Wang X and Liu XS. 2011. Systematic curation of miRBase annotation using integrated small RNA high-throughput sequencing data for *C. elegans* and *Drosophila*. *Front Genet* 2: 25.

Wang ZM, Zhang J, Ying Z and Heymsfield SB. 2012. Organ-tissue level model of resting energy expenditure across mammals: new insights into Kleiber's Law. *ISRN Zool*: 673050 (1-9).

White CR. 2011. Allometric estimation of metabolic rates in animals.
Comp Biochem Physiol A 158: 346-357.

White CR, Marshall DJ, Alton LA, Arnold PA, Beaman JE, Bywater CL, Condon C, Crispin TS, Janetzki A, Pirtle E, Winwood-Smith HS, Angilletta MJ, Chenoweth SF, Franklin CE, Franklin CE, Halsey LG, Kearney MR, Portugal SJ and Ortiz-Barrientos D. 2019. The origin and maintenance of metabolic allometry in animals. *Nature Ecol Evol* 3: 598-603.

White CR, Phillips N and Seymour R. 2006. The scaling and temperature dependence of vertebrate metabolism. *Biol Lett* 2: 125 – 127.

White CR and Seymour RS. 2005. Allometric scaling of mammalian metabolism.
J Exp Biol 208: 1611-1619.

Wright NA, Gregory TR and Witt CC. 2014. Metabolic 'engines' of flight drive genome size reduction in birds. *Proc Roy Soc B* 281: 20132780.

Wright T, Davis RW, Pearson HC, Murray M and Sheffield-Moore M. 2021. Skeletal muscle thermogenesis enables aquatic life in the smallest marine mammal. *Science* 373: 223–25.

Yu Q, Kolomeisky AB and Igoshin. 2022. The energy cost and optimal design of networks for biological discrimination. *J Royal Soc Interface* 19: 20210883–83.

Zatulovsky E and Skotheim JM. 2020. On the Molecular Mechanisms Regulating Animal Cell Size Homeostasis. *Trends Genetics* 36: 360-372.

Zolotarov G, Fromm B, Legnini I, Ayoub S, Polese G, Maselli V, Chabot PJ, Vinther J, Styfhals S, Seuntjens E, Di Cosmo A, Peterson KJ and Rajewsky N. 2022. MicroRNAs are deeply linked to the emergence of the complex octopus brain. *Sci Adv* 8: eadd9938 (1-12).

Zhang G, Li C, Li Q et al. 2014. Comparative genomics reveals insights into avian genome evolution and adaptation. *Science* 346: 1311-1320.

Zhang J and Yang J. 2015. Determinants of the rate of protein sequence evolution.
Nature Rev Genet 16: 409-420.

Zhang Q and Edwards SV. 2012. The Evolution of Intron Size in Amniotes: A Role for Powered Flight?
Gen Biol Evol 4: 1033-1043.